

# FunGlass School 2019/part 2

Papradno, Novemeber 27—29, 2019

*ORGANIZING INSTITUTIONS:*



**FunGlass School 2019 / Part 2**

**Book of Abstracts**

**Papradno, 27- 29 November, 2019**

**SCIENTIFIC BOARD:** Dušan Galusek, Prof., DSc., Marek Liška, Prof., DSc.

**REVIEWERS:** Dušan Galusek, Prof., DSc., Marek Liška, Prof. DSc., Mária Chromčíková, Assoc.Prof., Robert Klement, Assoc.Prof., Alfonz Plško, Assoc. Prof., Dr. Martin Michálek, Dr. Jozef Kraxner

**Edited by** Vanda Mokrářová

ISBN 978-80-8075-900-1  
EAN 9788080759001

## Obsah

<a href="#">J. J. Velázquez</a> Dopant effects on the structure and optical properties of the NaREF <sub>4</sub> oxyfluoride glass-ceramics.....	1
<a href="#">A. Prnová</a> Thermal behavior and photoluminescence properties of Er and Nd doped Y <sub>2</sub> O <sub>3</sub> -Al <sub>2</sub> O <sub>3</sub> glasses.....	3
<a href="#">A. Akusevich</a> Preparation of Ce <sup>3+</sup> -doped phosphors by sintering of glass microspheres .....	5
<a href="#">P. Švančárek</a> White Light Emitting Y <sub>2</sub> O <sub>3</sub> Based Fluorescents Containing up to 4 at% Zn <sup>2+</sup> .....	7
<a href="#">M. Žitňan</a> From the Edison bulb to new LED lights: the use of new glass-ceramic materials for energy-saving light sources .....	10
<a href="#">M. Blaško</a> DFT study of the Au-C bond formation in gold implanted polyethylene.....	12
<a href="#">B. Singarapu</a> Transparent glass-ceramic materials synthesized by Spark Plasma Sintering (SPS) for photonic applications.....	13
<a href="#">M. Michálková</a> Spark plasma sintering of glass microspheres with YAG composition.....	15
<a href="#">Nibu G. P.</a> Synthesis and sintering of nanocrystalline Ce <sup>3+</sup> - doped yttria nanoparticles prepared by precipitation method.....	17
<a href="#">A. Talimian</a> Chemical Tempering of Flexible Glasses .....	19
<a href="#">J. Valúchová</a> Study of thermal behavior and PL properties of Yb <sub>2</sub> O <sub>3</sub> -Al <sub>2</sub> O <sub>3</sub> glass microspheres .....	20
<a href="#">R. Dagupati</a> Structure and properties analysis by the Associate Solutions Thermodynamic Model in BaO-P <sub>2</sub> O <sub>5</sub> glasses .....	22
<a href="#">K. Griebenow</a> Network Mediated Coupling in Phosphate Glasses.....	24
<a href="#">M. Mahmoud</a> Effect of nucleating agents on the characterization of basaltic glass ceramics .....	26
<a href="#">F. Munoz</a> Fundamentals of solid state Nuclear Magnetic Resonance and application to the structure of glasses.....	28
<a href="#">A. Lopez</a> Thermodynamic study of the structure and properties of Li <sub>2</sub> O-P <sub>2</sub> O <sub>5</sub> glasses.....	30
<a href="#">A. Plško</a> Spectral properties of inorganic-organic films on glass .....	32
<a href="#">K. Faturíková</a> The influence of preparation conditions for inorganic-organic nanocomposite layers on their hydrophobicity .....	34
<a href="#">M. Parchovianský</a> Investigation and preparation of PDC glass/ceramic coatings applied to different pre-treated stainless steel AISI441 substrates .....	35
<a href="#">N. Afsharimani</a> Sol-gel based hybrid coatings for corrosion protection of AA2024-T3 alloys.....	37
<a href="#">I. Parchovianská</a> High temperature oxidation behavior of AISI441 stainless steel and PDC coatings in synthetic air atmosphere.....	39
<a href="#">N. Kamble</a> Corrosion resistance hybrid sol gel coating: its synthesis and characterizations.....	41
<a href="#">J. Kraxner</a> Porous Bioactive Glass Microspheres Prepared by Flame Synthesis.....	43
<a href="#">A. Dasan</a> Method for producing 3D silicate based bioactive glass-ceramic scaffolds using digital light processing.....	45
<a href="#">B. Pecušová</a> Influence of aluminosilicates and their modified forms on properties of composite materials .....	47
<a href="#">M. Michálek</a> Mesoporous bioactive glass doped with therapeutic inorganic ions.....	49
<a href="#">D. Galúsková</a> Initial dissolution profile and kinetics of glasses for bio applications.....	50
<a href="#">S. Chen</a> Multi-targeted B and Co co-doped bioactive glass for angiogenesis.....	53

<a href="#">Z. Neščíková</a> Electrospun polycaprolactone membranes doped with bioactive glass nanoparticles for tissue regeneration.....	55
<a href="#">A. Švančárková</a> Dissolution process of Bioglass 45S5 in physiological and acidic environment.....	56

## Dopant effects on the structure and optical properties of the NaREF<sub>4</sub> oxyfluoride glass-ceramics

J.J. Velázquez<sup>1</sup>, G. Gorni<sup>2,3</sup>, R. Balda<sup>4,5</sup>, J. Fernández<sup>6</sup>, A. Durán<sup>2</sup> and M.J. Pascual<sup>2</sup>

<sup>1</sup>FunGlass - Centre for Functional and Surface Functionalized Glass, Alexander Dubček University of Trenčín, 911 50 Trenčín, Slovakia.

<sup>2</sup>GLaSS group, Ceramic and Glass Institute (ICV-CSIC), 28049, Madrid, Spain

<sup>3</sup>Alba Synchrotron Light Source, Cerdanoyla del Valles, Barcelona, 08290, Spain

<sup>4</sup>Applied Physic Department I, Superior School of Engineering, Pais Vasco University, 48013 Bilbao, Spain

<sup>5</sup>Materials Physics Center CSIC-UPV/EHU, 20018 San Sebastian, Spain

<sup>6</sup>Donostia International Physics Center, 20018 San Sebastian, Spain

### ABSTRACT

Rare-earth (RE) doped nanostructured oxyfluoride glass-ceramics (GCs), have been widely studied due to the low phonon energy environments of fluorides (300–400 cm<sup>-1</sup>) and the mechanical advantages of oxide glasses. The principal applications of these materials are in photonics, such as infrared and tunable phosphors [1], three-dimensional colour optical recording/displays, white light generation for ambient lighting, light frequency up-conversion lasers, and solar cells [2–4].

In order to develop RE doped nGCs with high emission efficiency, the key factor is to select an appropriate fluoride host. From the suitable crystalline hosts, NaREF<sub>4</sub> in the form of NaGdF<sub>4</sub> or NaLuF<sub>4</sub> have been considered as one of the excellent luminescent host matrices for various RE ions. They are used for photonics applications, such as up- and down- converter materials for sensitive in-vivo bioimaging [5,6]. On the other hand, the processing route is a key issue for a suitable preparation of these materials. The typical glass processing method is the melting–quenching (MQ). This synthesis method requires high melting temperatures with a limitation in the fluorine content. However, bulk materials and fibers can be easily obtained. Instead of most of the studies were performed on bulk samples, the possibility to prepare GC fibers is also becoming a hot-spot for novel optical materials.

In this work, 0.5Er<sup>3+</sup> and 0.5Er<sup>3+</sup>-yYb<sup>3+</sup> (y = 2, 4 mol%) doped transparent aluminosilicate oxyfluoride GCs with NaGdF<sub>4</sub> or NaLuF<sub>4</sub> nanocrystals ranging from 10 to 50 nm were obtained by the melt-quenching process and suitable thermal treatment in the different forms such as bulk and fibers. These last ones have been prepared for the NaLuF<sub>4</sub> samples by the rod-in-tube method and controlled crystallization. The crystallization process for both composition was investigated using X-ray diffraction and high resolution transmission electron microscopy among others, Fig. 1.

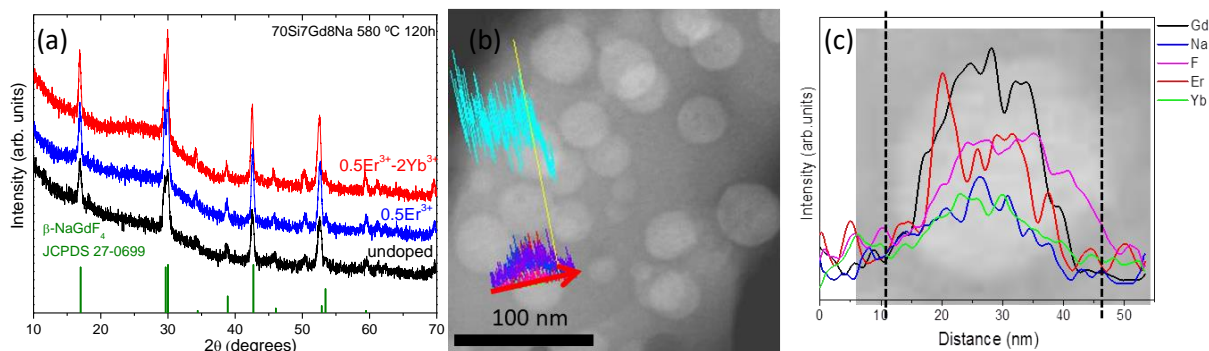


Fig.1 (a) XRD diffractograms for the un-doped, Er<sup>3+</sup> doped and Er<sup>3+</sup>-Yb<sup>3+</sup> co-doped d 70Si7Gd GC heat treated at 550 °C-120 h. (b) STEM-HAADF images of 0.5Er<sup>3+</sup>-2Yb<sup>3+</sup> co-doped GCs used for the EDX analysis and (c) its corresponding EDX line scan spectra of one nanocrystal.

Optical characterisation was also performed employing UV-Vis absorption spectra together with excitation and emission spectra. Excited state dynamics revealed the up-conversion (UC) mechanisms. Moreover, the UC emission color changes from yellow to green by increasing the excitation power density which allows to manipulate the color output of the  $\text{Er}^{3+}$  emission in the GCs. This tuneable emission color is easily detected with the naked eye and quantify by CIE chromaticity coordinates diagram, see Fig. 2. Finally, the relationship between processing-structure-optical properties of these materials is discussed as a function of the dopant concentration and the shape of the synthesized GCs.

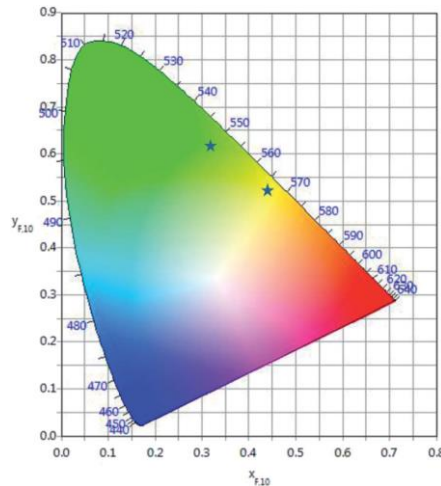


Fig.2. CIE chromaticity coordinates of the GC fiber for two different laser excitation densities, 2.5 and 0.75  $\text{kW cm}^{-2}$ , respectively.

**Keywords:** Glass-ceramic, Melting-quenching,  $\text{NaREF}_4$ , bulk and fibers, Up-conversion, Down-conversion.

### Acknowledgment:



This publication was created in the frame of the project Centre for Functional and Surface Functionalized Glass (CEGLASS), ITMS code is 313011R453, operational program Research and innovation, co-funded from European Regional Development Fund.

This work was also supported by MINECO under the project MAT2017-87035-C2-1-P/-2-P (AEI/FEDER, UE) and Basque Country University PPG17/07 and GIU17/014, and Basque Government PIBA2018-24. Funding from MPNS Cost Action MP1401 is also acknowledged.

### References:

- [1] Y. Wang and J. Ohwaki, *Appl. Phys. Lett.* 63(1993) 3268.
- [2] J.F. Suyver, J. Grimm, M.K. Van Veen, D. Biner, K.W. Krämer, H.U. Güdel, *J. Lumin.* 117(2006) 1.
- [3] T. Trupke, A. Shalav, B.S. Richards, P. Würfel and M.A. Green, *Sol. Energy Mat. Sol. Cells*, 90(2006) 3327.
- [4] A. de Pablos-Martín, M.O. Ramírez, A. Durán, L.E. Bausá, M.J. Pascual, *Opt. Mater.* 33(2010) 180.
- [5] Q. Liu, Y. Sun, T. Yang, W. Feng, C. Li, and F. Li, *J. Am. Chem. Soc.*, 133(2011) 17122–17125.
- [6] M.J. Pascual, C. Garrido, A. Miguel, L. Pascual, A. de Pablos-Martín, J. Fernández, R. Balda and A. Durán, *Int. J. App. Glass Sci.*, 7 (2016) 27–40.

## Thermal behavior and photoluminescence properties of Er and Nd doped $Y_2O_3-Al_2O_3$ glasses

**A. Prnová<sup>1</sup>, J. Valúchová<sup>2</sup>, M. Parchoviansky<sup>1</sup>, N. Mutlu, R. Klement, D. Galusek**

<sup>1</sup>*Vitrum Laugaricio Joint Glass Centre of the IIC SAS, TnUAD, FChPT STU, Študentská 911 50 Trenčín, Slovakia*

\* E-mail: [anna.prnova@tnuni.sk](mailto:anna.prnova@tnuni.sk)

<sup>2</sup>*FunGlass, A. Dubček University of Trenčín, Študentská 2, 911 50 Trenčín, Slovakia*

### ABSTRACT

Yttrium aluminate glasses (76.8 mol.% of  $Al_2O_3$ , 23.2 mol. % of  $Y_2O_3$ ) doped with  $Er^{3+}$  and  $Nd^{3+}$  ions at different concentration level (0.25 mol.%, 0.5 mol.% and 0.75 mol.%) were prepared by flame synthesis in the form of glass microspheres. The prepared samples were characterized by SEM (**Fig.1**) and XRD analysis. For study of thermal behavior of prepared systems, DSC analysis in temperature interval 35-1200°C, with heating rate 10°C/min was performed in nitrogen atmosphere. The list of prepared samples and basic properties are shown in (**Tab. 1**). The two exothermic effects ( $\approx 940$ ,  $\approx 1010^\circ C$ ) which can be assigned to crystallization of YAG phase in two steps were observed in DSC records of all prepared samples. The high temperature XRD measurements were performed in temperature interval 600-1200°C, with heating rate 5°C/min for more detailed study of thermal behavior of prepared systems and for study of temperature dependence of YAG content in samples during thermal treatment. In the whole temperature interval only YAG phase crystallization was observed. Based on excitation spectra of Er- and Nd- doped samples measured in the interval 250-750 nm, appropriate excitation wavelengths (380 nm for Er- and 360 nm for Nd- doped samples) were selected. The emission spectra were measured in VIS and NIR region in case of Er doped samples and in NIR region in case of Nd doped samples. All measured emission spectra (PL) (**Fig.2**) consist of characteristic bands due to the typical 4f-4f transitions in Er and Nd ions. From comparison of measured intensities it is evident, that the highest intensities were obtained for 0.5 mol. % Er doped sample (in both, NIR and VIS spectral regions). In the case of Nd doped samples, the maximum intensity value was found for the sample doped with 0.75 mol.% of Nd. The isothermal crystallization experiments at 1000°C and 1500°C were also performed with the dwell time of 20, 40 and 60 min. Measured emission spectra of crystallized samples shown slow increase of intensities in samples after 20 min annealing at 1000°C and Stark splitting of emission bands in samples after 40 and 60 min annealing at 1000°C and after 20, 40 and 60 min annealing at 1500°C, whereas further increase of splitted emission bands intensities was not observed.

From comparison of emission spectra of samples annealed at 1000°C for 40 and 60 min and emission spectra of samples annealed at 1500°C for 20, 40 and 60 min can be assumed, that the crystallisation of  $\alpha-Al_2O_3$  has no significant influence on the PL properties of crystallised microspheres[1].

**Tab.1:** The list of the samples and their basic characteristics

sample	$Al_2O_3$ [mol.%]	$Y_2O_3$ [mol.%]	$Er_2O_3$ [mol.%]	$Nd_2O_3$ [mol.%]	$T_{p1}$ [°C]	$T_{p2}$ [°C]	XRD
A6Y4Nd0.25	76.8	22.95	0.00	0.25	941	1010	amorphous
A6Y4Nd0.50	76.8	22.70	0.00	0.50	941	1011	amorphous
A6Y4Nd0.75	76.8	22.45	0.00	0.75	940	1012	amorphous
A6Y4Er0.25	76.8	22.95	0.25	0.00	941	1008	amorphous
A6Y4Er0.50	76.8	22.70	0.50	0.00	941	1008	amorphous
A6Y4Er0.75	76.8	22.45	0.75	0.00	941	1012	amorphous

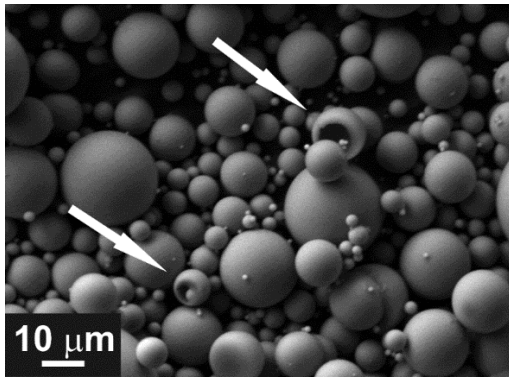


**Fig.1** SEM micrograph of AYE-Er0.5 prepared microspheres. The hollow microspheres are marked by arrows.

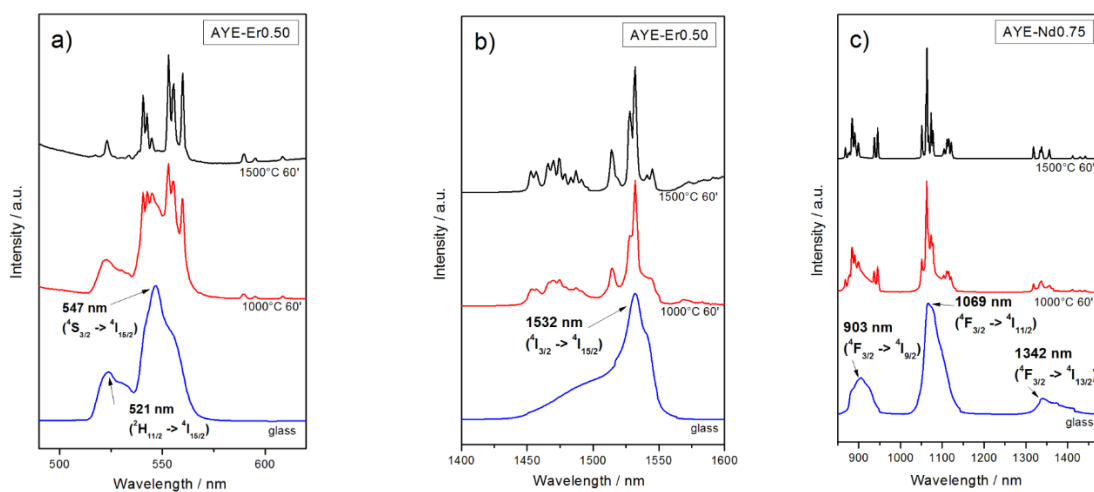


**Fig.2** The comparison of luminescence spectra measured in VIS spectral region of glass. AYE-Er0.5 and glass AYE-Er0.5 crystallized at 1000°C and 1500°C for 60 min (a) and in NIR region (b). The comparison of luminescence spectra measured in NIR region of glass AYE-Nd0.75 and glass AYE-Nd0.75 crystallized at 1000°C and 1500°C for 60 min (c).

## References

[1] A. Prnová, J. Valúchová, N. Mutlu M. Parchoviansky, R. Klement, A. Plško, D. Galusek, *Thermal behaviour and photoluminescence properties of Er and Nd doped yttrium aluminate glasses*, *Journal of Thermal Analysis and Calorimetry*, submitted.

## Acknowledgments



This paper is a part of dissemination activities of project FunGlass. This project has received funding from the European Union's Horizon 2020, research and innovation programme under grant agreement No 739566. The financial support of this work by the projects APVV 0014-15, VEGA 1/0527/18, APVV-17-0049, VEGA 2/0026/17, VEGA 2/0088/16 and VEGA 1/0064/18 is gratefully acknowledged.

## Preparation of Ce<sup>3+</sup>-doped phosphors by sintering of glass microspheres

**A. Akusevich<sup>1</sup>, I. Parchovianská<sup>1</sup>, M. Parchovianský<sup>2</sup>, A. Prnová<sup>3</sup>, R. Klement<sup>1</sup>**

<sup>1</sup> Department of Functional Materials, FunGlass, Alexander Dubček University of Trenčín, Študentská 2, 911 50 Trenčín, Slovakia (E-mail:alena.akusevich@tnuni.sk)

<sup>2</sup> Department of Coating Processes, FunGlass, Alexander Dubček University of Trenčín, Študentská 2, 911 50 Trenčín, Slovakia

<sup>3</sup> Join Glass Centre of the IIC SAS, TnUAD, FChPT STU, Študentská 2, 911 50 Trenčín, Slovakia

### ABSTRACT

In the present work we report on preparation and preliminary characterisation of compact samples prepared by hot pressing of glass microspheres powders in the Ce<sup>3+</sup> doped Y<sub>2</sub>O<sub>3</sub>-Al<sub>2</sub>O<sub>3</sub> system with different ratio of YAG to Al<sub>2</sub>O<sub>3</sub> phase in a composite. First, the thermal properties of prepared glass microspheres were studied by differential scanning calorimetry (DSC). Based on the thermal behaviour, the hot press conditions were selected and luminescent properties of prepared compacts have been investigated.

The composition of prepared Ce<sup>3+</sup>-doped glasses is derived from the corresponding un-doped system by equimolar substitution of Y<sub>2</sub>O<sub>3</sub> by Ce<sub>2</sub>O<sub>3</sub> and is summarised in Tab. 1. The concentration of Ce<sup>3+</sup> ions in a glass was kept at constant level of 1.0 at.%.

**Tab. 1:** Theoretical composition of prepared glass

Sample <sup>&amp;</sup>	Glass composition				
	Y <sub>2</sub> O <sub>3</sub> (mol.%)	Al <sub>2</sub> O <sub>3</sub> (mol.%)	Ce <sub>2</sub> O <sub>3</sub> (mol.%)	Ce <sup>3+</sup> (at.%)	Ce <sup>3+</sup> in YAG (at.%) <sup>#</sup>
30% YAG : 70% Al <sub>2</sub> O <sub>3</sub> (eut.)	22.64	76.86	0.50	1.00	3.48
50% YAG : 50% Al <sub>2</sub> O <sub>3</sub>	18.25	81.25	0.50	1.00	2.00
70% YAG : 30% Al <sub>2</sub> O <sub>3</sub>	25.75	73.75	0.50	1.00	1.42

<sup>&</sup>Denotes composition of YAG/Al<sub>2</sub>O<sub>3</sub> phase in the whole sample in mol.%; <sup>#</sup>Recalculated under assumption that all Ce<sup>3+</sup> ions are hosted in YAG phase after crystallization (heat treatment).

The prepared glass microspheres of given compositions were found to be XRD amorphous within the detection limit of the XRD diffractometer. The DSC analysis revealed the two exothermic effects, the first one at temperatures around 940°C and the second effect, ranging from 965°C up to 1060°C, that is significantly dependent on the composition of the glass. Both effects correspond to the crystallization of the YAG phase, as documented also by high temperature XRD [1]. The Al<sub>2</sub>O<sub>3</sub> phase as corundum start to crystallize over 1300°C [1]. The *T<sub>g</sub>* temperature estimated from DSC data was found to be around 890°C.

The bulk glass from microspheres with eutectic composition was prepared at temperature 840°C with dwell time 0 min, applying the pressure of 40MPa. The glass-ceramic samples with YAG crystals embedded in residual glass matrix were prepared at temperatures 1000°C and 1100°C with the dwell time 30 and 60 min. The yellow colour of the consolidated bulk samples typical for the YAG:Ce phosphor was observed. It should be noted, that for hot-press experiments, glass microspheres without any treatment in reducing atmosphere was used.

The excitation (PLE) and emission (PL) spectra of the glass bulk sample with eutectic composition is depicted on Fig. 1A. The excitation spectrum was monitored at wavelength 430 nm. The strong absorption with maxima at 355 nm can be ascribed to 4f-5d transition in Ce<sup>3+</sup> ions. The emission spectrum of the glass compact recorded under UV excitation at 350 nm exhibits broad emission band in spectral range of 365-550 nm with the emission maximum at 430 nm. This emission corresponds to the 5d→<sup>2</sup>F<sub>5/2</sub> and 5d→<sup>2</sup>F<sub>7/2</sub> transitions that are not clearly resolved as in the other Ce<sup>3+</sup> doped systems with blue emission [2]. This is most likely due to the close energy of the 4f (<sup>2</sup>F<sub>5/2</sub>, <sup>2</sup>F<sub>7/2</sub>) ground states in Ce<sup>3+</sup> ions in the yttrium aluminate glass; Ce<sup>3+</sup> with 4f<sup>1</sup> electron configuration has two ground states of <sup>2</sup>F<sub>5/2</sub> and <sup>2</sup>F<sub>7/2</sub> due to the spin-orbital coupling. The blue emission point to the weaker crystal field strength around Ce<sup>3+</sup> ions in prepared glasses compared

to the crystal field strength around  $\text{Ce}^{3+}$  ions in YAG phase (green-yellow emission).

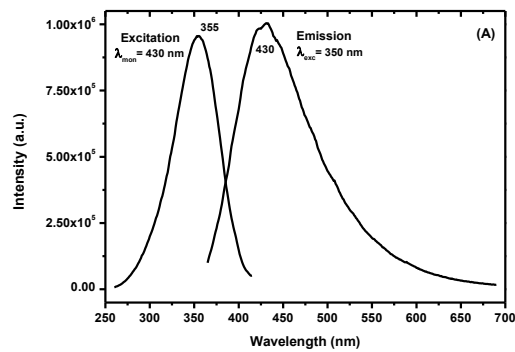
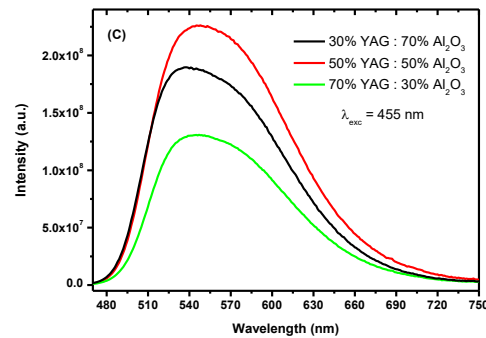
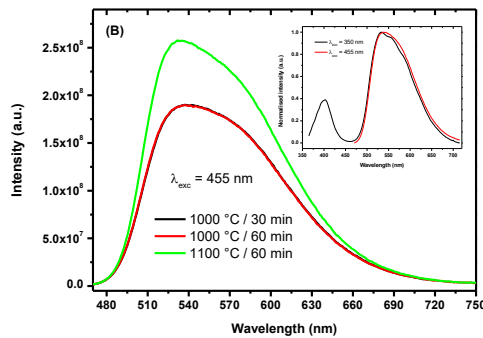


Fig. 1: (A) The excitation and emission (PL) spectra of sample with composition 30% YAG-70%  $\text{Al}_2\text{O}_3$  (eutectic composition) prepared by hot-press of glass microspheres at  $840^\circ\text{C}/0$  min. (B) The PL spectra of sample with composition 30% YAG-70%  $\text{Al}_2\text{O}_3$  prepared by hot-press of glass microspheres at different temperature and dwell time. Inset represent emission spectra under sample excitation by UV and blue light. (C) The PL spectra of sample with different composition prepared by hot-press of glass microspheres at  $1000^\circ\text{C}/60$  min.



The PL emission spectra ( $\lambda_{\text{exc}} = 455$  nm) of hot-pressed samples with eutectic composition at different temperatures and dwell time are depicted in Fig. 1B. A typical broad emission band centred at  $\sim 550$  nm is seen in spectra of samples. The PL emission curves can be deconvoluted into two broad Gaussian bands centred at  $\sim 527$  nm (peak 1) and  $\sim 577$  nm (peak 2). These two peaks correspond to the typical  $5d^1-4f^1$  ( ${}^2F_{5/2}$ ) and  $5d^1-4f^1$  ( ${}^2F_{7/2}$ ) transitions of  $\text{Ce}^{3+}$  ion, the energy difference between the two energy levels is  $\sim 1600$   $\text{cm}^{-1}$  due to of the spin-orbital coupling in crystal-field [3]. The PL emission intensity depends on the treatment temperature. As the temperature increases from  $1000^\circ\text{C}$  to  $1100^\circ\text{C}$ , the PL emission intensity significantly increases. The increase of emission intensity with treatment temperature is due to the improvement of crystallinity of samples; most likely more  $\text{Ce}^{3+}$  doped YAG crystalline phase is formed in the residual glass matrix. The PL spectra of compact samples prepared from different compositions of starting glass sintered at  $1000^\circ\text{C}/60$  min are depicted in Fig. 1C. The emission intensity increases with expected concentration of  $\text{Ce}^{3+}$  ions in YAG phase for 1.42 and 2.0 at.%, than for concentration 3.48 at.% decreases, most likely due to the energy transfer between  $\text{Ce}^{3+}$  ions and non-radiative transitions, the effect well known as concentration quenching. The testing of mechanical properties and microstructural study of compact bulk phosphors is currently in progress.

**Keywords:**  $\text{Ce}^{3+}$ , phosphors, solid state lighting, pc-WLED.

### Acknowledgment:



This item is a part of dissemination activities of project [FunGlass](#). This project has received funding from the European Union's Horizon 2020 research and innovation programme under grant agreement No 739566. This work was also supported by the Slovak Research and Development Agency under the contract No. APVV-17-0049 and by grant VEGA 1/0527/18.

### References:

- [1] A. Prnová, R. Klement, K. Bodišová, J. Valúchová, D. Galusek, E. Bruneel, I.V. Driessche, Thermal behaviour of yttrium aluminate glasses studied by DSC, high-temperature X-ray diffraction, SEM and SEM EDS, *J. Therm. Anal. Calorim.* 128 (2017) 1407-1415.
- [2] G. Zhu, Z. Ci, Q. Wang, Y. Wen, S. Han, Y. Shi, S. Xin and Y. Wang, *J. Mater. Chem. C*, 1 (2013) 4490-4496.
- [3] R.R. Jacobs, W.F. Krupke and M.J. Weber, *Appl. Phys. Lett.* 33 (1978) 410-412.

# White Light Emitting $Y_2O_3$ Based Fluorescents Containing up to 4 at% $Zn^{2+}$

P. Švančárek<sup>1</sup>, R. Klement<sup>2</sup>, M. Parchoviansky<sup>2</sup> and D. Galusek<sup>1,2</sup>

<sup>1</sup> Joint Glass Centre of the IIC SAS, TnUAD, FChPT STU, FunGlass, Študentská 2, 911 50 Trenčín, Slovakia

<sup>2</sup> Centre for Functional and Surface Functionalized Glass, Alexander Dubcek University of Trenčín, 911 50 Trenčín, Slovakia

(E-mail: peter.svancarek@tuni.sk)

## ABSTRACT

In this work we investigated fluorescence activity of yttria ceramic materials modified by various amounts of ZnO. The  $Y_2O_3$  green bodies were prepared by pressure filtration of isopropanol ( $(CH_3)_2CHOH$ , p.a., 99.7%+, CentralChem, Slovakia) based suspension containing 5 vol% of  $Y_2O_3$  (PENGDA, 150 nm), stabilized by 1 wt.% of PEG (Polyethylene Glycol 400 Ultra-pure, Fluka, Germany) based on the  $Y_2O_3$  mass. After drying, the green pellets were pre-sintered using the following regime: ramp  $10^\circ C/min$  to  $1000^\circ C$  with 1 hour holding time followed by free cooling in furnace as to obtain porous but sufficiently stable pellets able to withstand infiltration procedure in water based solutions.

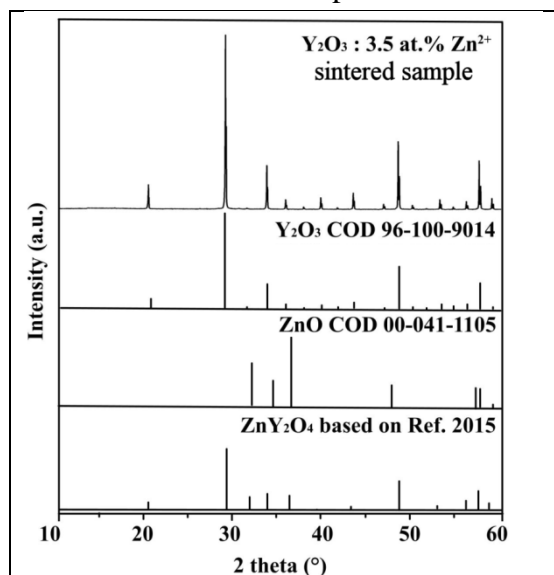


**Fig. 1.** XRD pattern acquired from a sintered sample along with the theoretical patterns of  $Y_2O_3$ , ZnO and phase of the proposed composition  $ZnY_2O_4$  described in Ref. [1]

Water solutions of zinc acetate ( $Zn(CH_3COO)_2 \cdot 2H_2O$  p.a., CentralChem, Slovakia) with concentrations calculated individually according to porosity of pre-sintered pellets to obtain 0.25, 0.5, 1.0, 2.0, 3.0, 3.5 and 4 atomic percent of  $Zn^{2+}$  dopant were used for infiltration of pre-sintered pellets. The infiltrated pellets were then sintered in ambient atmosphere using superkanthal furnace (Classic, Czech republic) using the following regime: ramp  $10^\circ C/min$  to  $80^\circ C$  with 2 hours holding time, then ramp  $10^\circ C/min$  to  $250^\circ C$  with 2 hours holding time and finally, ramp  $10^\circ C/min$  to  $1400^\circ C$  with 2hour holding time followed by free cooling. To confirm the role of vacancies on fluorescence intensities, the final sintering step temperatures  $1300^\circ C$  and  $1500^\circ C$  were also used for the sample compositions with the strongest fluorescence activity.

X-ray diffraction (XRD) was performed using a PANalytical Empyrean DY1098 X-ray powder diffractometer with  $CuK\alpha$ -radiation in the  $\theta$ - $2\theta$  arrangement. Fig.1 The only detected phase was  $Y_2O_3$ .

Cross sections for SEM were prepared by cutting the pellets in half and embedding them in Buehler KonductoMet (pressure molding at  $150^\circ C$  for 1 min). The cross sections were ground and polished on diamond wheels using decreasing grain sizes from  $45\mu m$  down to  $0.5\mu m$  in a Buehler AutoMet 300 polisher. A final finish of 2-6 h of vibration polishing was applied using a Buehler VibroMet 2 (200 g static load) and a MasterPrep polishing suspension

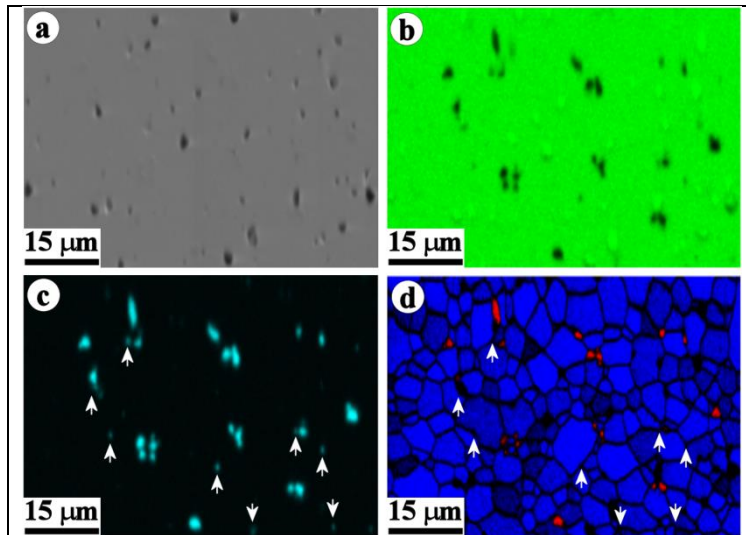


**Fig. 2.** a) SEM micrograph of the sintered ceramic. EDXS element maps of b) Y and c) Zn are presented along with d) the phase map of an EBSD scan performed on the area. White arrows highlight locations where elevated levels of Zn are detected by EDXS but which did not provide EBSD-patterns indexed as ZnO during the EBSD-scan.

1.38  $\mu\text{m}$  contain discreet ZnO grains distributed in a matrix of  $\text{Y}_2\text{O}_3$ . No other  $\text{Zn}^{2+}$  containing phases were detected. EBSD-pattern superposition can lead to mis-indexed EBSD-patterns when using the applied software package. The existence of a proposed phase [Chyba! Záložka nie je definovaná.] with the composition  $\text{ZnY}_2\text{O}_4$  is questionable.

Both emission (PL) and excitation (PLE) fluorescence spectra were measured using a Fluorolog 3 (FL3-21, Horiba) fluorescence spectrometer in the front-face mode with a Xe-lamp (450 W) as the excitation source. Fig.3.

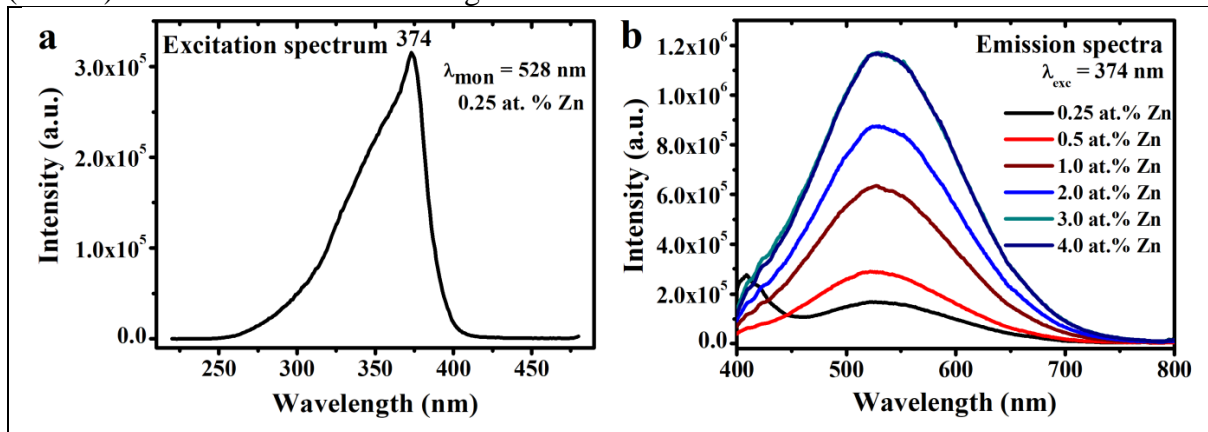


**Fig. 3.** a) Excitation (PLE) and b) emission (PL) spectra of  $\text{Y}_2\text{O}_3$  ceramics containing  $\text{Zn}^{2+}$  sintered for 2 h at  $1400\text{ }^\circ\text{C}$

The produced ceramics show a strong emission in a broad range of electromagnetic wavelengths in the visible part of spectrum with maximum around 534 nm. The observed photoluminescence is attributed to a mechanism described for the system ZnO:Zn due to similarities in the luminescence spectra. [2]

**Keywords:** Fluorescence, Pressure filtration,  $\text{Y}_2\text{O}_3$  ceramics, ZnO

**Acknowledgment:**

This item is a part of dissemination activities of project [FunGlass](#).

This project has received funding from the European Union's Horizon 2020 research and innovation programme under grant agreement No 739566.

This work was also supported by the Slovak Research and Development Agency under the contract No. APVV-17-0049 and by grants VEGA 1/0527/18, VEGA 2/0026/17.

We also wish to thank Dr. Wolfgang Wisniewski for his help with EBSD measurements.

**References:**

<sup>1</sup> Bidhu Bhusan Das, Venugopal Potu and Govinda Rao Ruppá: Synthesis, crystal structure and magnetic studies of ZnY<sub>2</sub>O<sub>4</sub> oxide, Indian Journal of Pure & Applied Physics Vol. 53, pp. 399-403, 2015

<sup>2</sup> P. A. Rodnyi, K. A. Chernenko, and I. D. Venevtsev: Mechanisms of ZnO Luminescence in the Visible Spectral Region, Optics and Spectroscopy, 2018, Vol. 125, No. 3, pp. 372–378. 2018

## From the Edison bulb to new LED lights: the use of new glass-ceramic materials for energy-saving light sources

**M. Žitňan<sup>1</sup>, J. Velázquez García<sup>1</sup>, M. Blaško<sup>1</sup>, F. Lofaj<sup>2</sup> and D. Galusek<sup>1</sup>**

<sup>1</sup> FunGlass, Alexander Dubcek University of Trencin, Studentska 2, 91150 Trenčín, Slovakia

(E-mail: [michal.zitnan@tuni.sk](mailto:michal.zitnan@tuni.sk))

<sup>2</sup> Institute of Materials Research, Slovak Academy of Sciences, Watsonova 47, 040 01 Košice, Slovakia

### ABSTRACT

Since the first electric light invented in 1802 the electric bulbs passed through noticeable technological advance, most visible in the increase of energy-to-light efficiency that has grown from 5 to 90%. In 1880 the first incandescent bulb with filament based on carbonized bamboo was commercially successful. Since 1950s the quartz glass and halogen light bulb have been produced. In 1970s compact fluorescent bulb with spiral shape was invented. After the development of GaN blue diode, white light LED (Light Emitting Diode) sources appeared. The bulbs encapsulate InGaN blue LED covered by yellow phosphor. Common yellow phosphor material is cerium-doped yttrium aluminium garnet ( $\text{Ce}^{3+}:\text{YAG}$ ). The most efficient phosphors use rare-earth elements as dopants. After China, the main producer of rare-earths, limited exports of these materials in 2009 and 2010, a price spike occurred on stock market. After this event, there is demand on white light sources with limited content of rare-earths. One option how to overcome this issue is to use RE-free materials, mainly doped with transition metals, such as Ag, Au, Mn, Cu, Cr, Fe [1-3].

The special interest is the use of glass-ceramics that comprise wide band-gap semiconductor nanocrystals, dispersed in a glassy matrix, for a suitable application in LEDs. These nanocrystals strongly absorb photons with energies larger than their gap and transfer this energy very efficiently to lanthanide or metal transition ions. The inter-band excitation of these nanoparticles can lead to very efficient emission of doping agents by means of energy transfer. Moreover, the quantum confinement due to the nanocrystals sizes enhances the energy transfer efficiency increasing the luminescence of these systems. This efficiency is even higher in the wide band-gap semiconductors such as  $\text{SnO}_2$ ,  $\text{TiO}_2$  or  $\text{ZnO}$ , with an energy gap over 3.0 eV, compared to others such as Si or GaAs with energy gap around 1 eV [4]. Our aim is to design, synthesize, and characterize systems based on wide band-gap semiconductors.  $\text{SnO}_2$ ,  $\text{TiO}_2$  and  $\text{ZnO}$  has been selected with an energy gap over 3 eV.  $\text{SnO}_2$  is an *n*-type semiconductor with a gap 3.6 eV at 300 K and it is well-known due to the potential applications in solar cells, transparent conductive electrodes and catalysis. Several works have been published related to glass-ceramics based on  $\text{SnO}_2$  nanocrystals precipitated in a glassy matrix of silica, obtained by sol-gel method and after adequate heat treatments. Chioldini et al. [5] analyzed the broadening of the gap through the analysis of the nanocrystals size distribution, and correlate them with the quantum confinement of the nanocrystals.

Regarding  $\text{TiO}_2$ , this semiconductor is attracting increasing attention in the decades as a host wide-gap semiconductor, with the high refractive index and high transparency in the visible and infrared regions. The additional advantages of using  $\text{TiO}_2$  are its low fabrication cost and good thermal and mechanical stabilities. Moreover, it is an environmentally-friendly material and is generally considered non-toxic, so can not only be used as a host for luminescence and applied to LEDs and other optoelectronic devices, but can also be applied to solar cells, photocatalysts and other energy-related products [6-9].

Finally, Zinc oxide with a wide bandgap of 3.37eV has been known for efficient and bright luminescence for many years [10]. Having large exciton binding energy of  $\sim 60$  meV, it served as a model system for understanding the properties of excitons [11,12]. The advantages of  $\text{ZnO}$  include the ability to lase as thin films [13], as random crystallites [14] and in nanostructured form [15].

Our aim is to determine the relationship between chemical composition, structure and the wavelength of the emitted light. This allows us to develop novel rare-earth free yellowish and blue

light-emitting diodes based on wide band-gap semiconductors with enhancing emissivity in yellow and blue spectrum range.

**Keywords:** dopant, glass-ceramics, LED, rare-earth free, semiconductor, wide band-gap

**Acknowledgment:**



This publication was created in the frame of the project Centre for Functional and Surface Functionalized Glass (CEGLASS), ITMS code is 313011R453, operational program Research and innovation, co-funded from European Regional Development Fund.

**References:**

- [1] F. Kreller, J. Puls, and F. Henneberger: *Appl. Phys. Lett.* 69 (1996) 2406
- [2] J.W. Park, J.O. Song, D.S. Leem, and T.Y. Seong: *Electrochem. Solid State Lett.* 8 (2005) G17
- [3]. H.W. Jang and J.L. Lee: *Appl. Phys. Lett.* 85 (2004) 4421
- [4] N. Chiodini, A. Paleari, D. Di Martino y G. Spinolo, *Appl. Phys. Lett.* 81, (2002) 1702
- [5] N. Chiodini, A. Paleari, G. Brambilla y E.R. Taylor, *Appl. Phys. Lett.* 80, (2002) 4449
- [6] Shi, E., Zhang, L., Li, Z., Li, P., Shang, Y., Jia, Y., Wei, J., Wang, K., Zhu, H., Wu, D., Zhang, S. and Cao, A. *Scientific Reports*, 2, (2012), Article No. 884
- [7] Holland, L., Laurenson, L., Baker, P.N. and Davis, H.J. *Nature*, 238, (1972) 37-38
- [8] Fujishima, A., Zhang, X. and Tryk, D.A. *Surface Science Reports*, 63 (2008) 515-582
- [9] Murayama, M., Yoda, K. , Shiraishi, K. , Guan, S. , Komuro, S. and Zhao, X. *Optics and Photonics Journal*, 8, (2018) 146-164
- [10] Ü. Özgür, Ya. I. Alivov, C. Liu, A. Teke, M. A. Reshchikov, S. Doğan, V. Avrutin, S.-J. Cho, and H. Morkoç *Journal of Applied Physics* 98, (2005) 041301
- [11] R.E. Dietz, J.J. Hopfield, D.G. Thomas, *Journal of Applied Physics*, 32, (1961) 2282
- [12] D.G. Thomas, J.J. Hopfield, *Physical Review Letters*, 7, (1961) 316
- [13] Bagnall, DM; Chen, YF; Zhu, Z; et al. *Applied Physics Letters* 70 (1997) 2230-2232
- [14] H Cao, YG Zhao, HC Ong, ST Ho, JY Dai, JY Wu, RPH Chang - *Applied Physics Letters*, 1998
- [15] Huang, MH; Mao, S; Feick, H; Yan, HQ; Wu, YY; Kind, H; Weber, E; Russo, R; Yang, PD, *Science* 292 (2001) 1897-1899

## DFT study of the Au-C bond formation in gold implanted polyethylene

Andrej Antušek<sup>1</sup>, Martin Blaško<sup>2</sup>, Miroslav Urban<sup>2</sup>, Pavol Noga<sup>1</sup> and Miloš Nenadović<sup>3</sup>

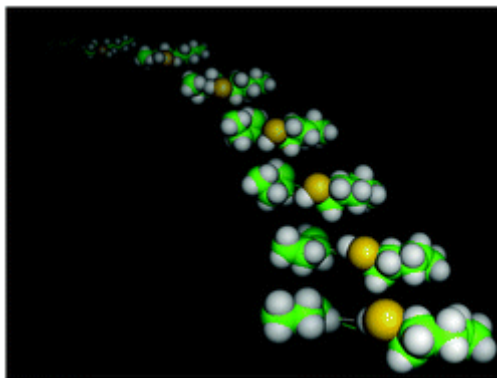
<sup>1</sup>ATRI, Faculty of Materials Science and Technology in Trnava, ATRI, Slovak University of Technology in Bratislava, J. Bottu 25, 917 24 Trnava, Slovak Republic

<sup>2</sup>Department of Physical and Theoretical Chemistry, Faculty of Natural Sciences, Comenius University, Ilkovičova 6, Mlynská dolina, 84215 Bratislava, Slovak Republic (blasko25@fns.uniba.sk)

<sup>3</sup>INS Vinča, Laboratory of Atomic Physics, Mike Alasa 12-14, Belgrade, Serbia

### ABSTRACT

The processes of the gold implantation into the polyethylene (PE) were studied theoretically on the DFT (Density Functional Theory) level. First, smaller fragments consisting of 5 to 15 carbon atoms were used for basic insight into PE implanted by Au. The Car-Parrinello molecular dynamics was applied for the modeling of collisions of Au<sup>+</sup>, Au and AuH with PE. Based on CCSD(T) benchmarks and previous studies on small Au<sub>n</sub>-ligand clusters [1], thermodynamic data and IR spectra of possible Au containing PE fragments were calculated using DFT/PBE0 method. Basic motifs are described as H atom of PE substituted by gold, Au serving as a C-Au-C bridge connecting two PE fragments and Au incorporated in the backbone structure of PE. The NBO analysis reveals the covalent character of C-Au bonds with binding energies of about 200 kJ/mol. Calculated IR spectra helped to assign experimental FTIR spectra of HDPE before and after Au implantation, employing methods described in Ref. [2]. Most significant indication of Au implanted in PE are stretching C-Au vibrations lying around 500 cm<sup>-1</sup> and a broad band (in range of 730 - 1300 cm<sup>-1</sup>) IR active in PE implanted by Au.



**Keywords:** DFT, FTIR, gold, HDPE, molecular dynamics

**Acknowledgments:** We thank for the support from following grants APVV-15-0105, VEGA 1/0465/15, ERDF "Univ. Sci. Park Campus MTF STU - CAMBO" ITMS: 2622022017 and project No. 003STU-2-3/2016.

### References

- [1] M. Blasko, T. Rajskey, M. Urban, Chem. Phys. Lett., 671, 84 (2017).
- [2] M. Nenadovic, J. Potocnik, M. Mitric, S. Strbac, Z. Rakocevic, Mat. Chem. Phys., 142, 633(2013).

# Transparent glass-ceramic materials synthesized by Spark Plasma Sintering (SPS) for photonic applications

**S. Babu<sup>1,2\*</sup>, R. Balda<sup>3,4</sup>, J. Fernández<sup>5</sup>, M. Sedano<sup>2</sup>, D. Galusek<sup>1, 6</sup>, A. Durán<sup>2</sup>, M.J. Pascual<sup>2\*</sup>**

<sup>1</sup>FunGlass, Alexander Dubček University of Trenčín, Študentská 2, 911 50 Trenčín, Slovakia

<sup>2</sup>Instituto de Cerámica y Vidrio (ICV-CSIC), 28049, Madrid, Spain

<sup>3</sup>Dept. Física Aplicada I, Escuela Superior de Ingeniería, Universidad del País Vasco (UPV-EHU), 48013 Bilbao, Spain

<sup>4</sup>Centro de Física de Materiales, (UPV/EHU-CSIC), 20018 San Sebastian Spain

<sup>5</sup>Donostia International Physics Center DIPC, 20018 San Sebastian, Spain

<sup>6</sup>Joint glass centre of the IIC SAS, TnUAD, and FChFT STU, FunGlass, Alexander Dubček University of Trenčín, 911 50 Trenčín, Slovakia

(E-mail: babu.singarapu@tnuni.sk, mpascual@icv.csic.es)

## ABSTRACT

### 1 Introduction

Transparent glass-ceramic materials combine thermal stability and good optical properties compared to single crystals, high mechanical properties and low manufacturing costs [1]. Spark Plasma Sintering (SPS) is an alternative processing method to prepare transparent glass-ceramic materials. SPS combines uniaxial pressure and heating based on the Joule effect, and offers the possibility of sintering powders up to full density [2]. However, various extrinsic and intrinsic factors affect transparency of glass-ceramics. Some extrinsic factors are the processing parameters such as particle size of the glass powder, temperature, time and pressure. Intrinsic factors are carbon contamination, pores and secondary phases.

Glass-ceramics of the  $\text{Li}_2\text{O}-\text{Al}_2\text{O}_3-\text{SiO}_2$  (LAS) system [3] with very low thermal expansion have been successfully obtained by SPS. Delaizir et al. [4] used SPS for the preparation of  $62.5\text{GeS}_2-12.5\text{Sb}_2\text{S}_3-25\text{CsCl}$  glass-ceramics in order to reduce the sintering time compared with conventional sintering. Laure et al. [5] reported sintered soda-lime glass microspheres by SPS. In all these works, the SPS experiments had to be carefully optimized with respect to temperature, time and pressure. The main objectives of this paper is the preparation of transparent GCs containing low phonon fluoride phases such as  $\text{KLaF}_4$  &  $\text{NaLaF}_4$  by controlling the processing parameters, namely particle size of the glass powder, pressure, temperature and holding time. Carbon contamination was avoided by using platinum foil. Final materials with low porosity, nanometer-sized crystals dispersed within the glassy matrix and high transparency have been prepared.

### 2 Experimental

Glasses with compositions  $70\text{SiO}_2-7\text{Al}_2\text{O}_3-16\text{K}_2\text{O}-7\text{LaF}_3$  (mol%) and  $70\text{SiO}_2-7\text{Al}_2\text{O}_3-8\text{Na}_2\text{O}-8\text{K}_2\text{O}-7\text{LaF}_3$  (mol%) doped with different concentrations of  $\text{NdF}_3$  (0.1 and 0.5 mol%) and  $\text{TmF}_3$  (0.1, 0.5 and 1.0 mol%), respectively, were prepared by melt-quenching method at temperatures between 1600-1650°C. The glasses were milled and the glass powders sieved to obtain fractions <40  $\mu\text{m}$ , <63  $\mu\text{m}$ , and 63-100  $\mu\text{m}$ . Pellets were prepared applying a pressure of 2000KPa and sintered under vacuum, using optimized SPS processing parameters such as temperature, pressure and holding time in a DR. SINTER SPS-510CE. Pulsed direct current (pulses of 12 ms on/2 ms off) was applied. The temperature was measured by an optical pyrometer focused on a hole in the graphite die.

### 3 Results and Discussion

The SPS optimum processing parameters were found to be: temperature- 700°C, pressure- 22MPa, holding time-10 to 20 min. Carbon contamination originating from the graphite dies employed in the SPS experiments was observed. Contamination could be eliminated by using platinum foil to cover the samples inside the die.

The prepared oxyfluoride GCs exhibited high stability and transparency. Similarly, NaLaF<sub>4</sub>: Tm<sup>3+</sup> 0.1, 0.5 and 1.0 mol% doped transparent GCs were obtained by SPS. Fig. 1 shows the XRD patterns for the KLaF<sub>4</sub> ( $\alpha$  and  $\beta$ ) glass-ceramics. The size of the crystals being in the range ~19-23 nm for  $\alpha$ -KLaF<sub>4</sub>, using the Scherrer equation [2]. Transparency decreases with decreasing particle size of the used glass powder, as confirmed by the measurement of optical spectra in transmission mode.

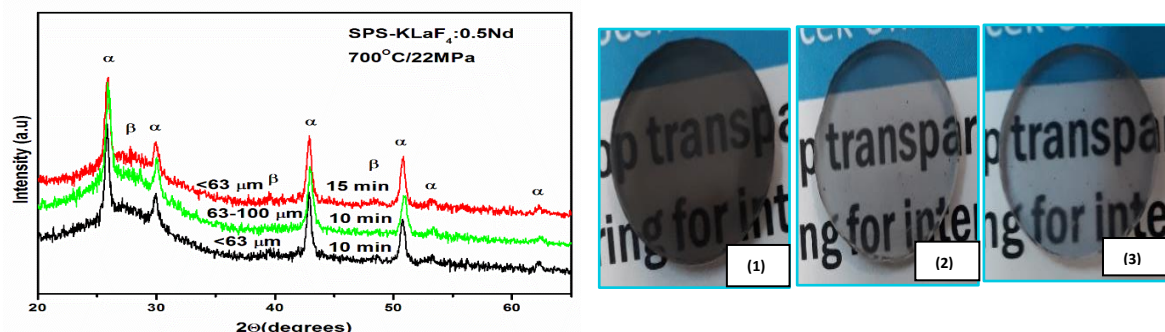


Fig. 1. XRD profile and appearance of KLaF<sub>4</sub> glass-ceramics: 0.5 mol% Nd doped TGCs from powders of different particle sizes (1) <40  $\mu\text{m}$  (2) <63  $\mu\text{m}$  (3) 63-100  $\mu\text{m}$

#### 4 Conclusion

Transparent oxyfluoride TGCs were successfully prepared by SPS. KLaF<sub>4</sub> and NaLaF<sub>4</sub> nanocrystals containing GCs were obtained by the optimized SPS process. The sintered samples were transparent in the visible wavelength range. The use of platinum foil, to cover pellets during SPS, effectively reduced carbon contamination.

**Keywords:** Spark Plasma Sintering; Transparent Glass-ceramics; KLaF<sub>4</sub>; NaLaF<sub>4</sub>; Photonics.

#### Acknowledgment:



This item is a part of dissemination activities of project [FunGlass](#).

This project has received funding from the European Union's Horizon 2020 research and innovation programme under grant agreement No 739566.

Funding from the project MAT2017-87035-C2-1-P/2-P (AEI/FEDER, UE) and VEGA 1/0527/18 are gratefully acknowledged.

#### References:

- [1] C. Xu, C. Yang, H. Zhang, Y. Duan, H. Zhu, D. Tang, H. Huang, J. Zhanga, *Opt. Express*, 24, 20571 (2016).
- [2] A.A. Cabral, R. Balda, J. Fernández, G. Gorni, J. J. Velázquez, L. Pascual, A. Durán, M. J. Pascual, *CrystEngComm*, 20, 5760 (2018).
- [3] P. Riello, S. Bucella, L. Zamengo, U. Anselmi-Tamburini, R. Francini, S. Pietrantoni, Z.A. Munir. *J. Eur.Ceram. Soc.*, 26, 3301 (2006).
- [4] G. Delaizir, M. Dolle, P. Rozier, *J. Am. Ceram. Soc.*, 93, 2495 (2010).
- [5] L. Ramond, G. Bernard-Granger, A. Addad, C. Guizard, *J. Am. Ceram. Soc.*, 94, 2926 (2011).

## Spark plasma sintering of glass microspheres with YAG composition

**Monika Micháľková<sup>1</sup>, Jozef Kraxner<sup>2</sup>, Václav Pouchlý<sup>3</sup>, Karel Maca<sup>3</sup>, Dušan Galusek<sup>2</sup>**

<sup>1</sup> Dpt. VILA – Joint Glass Centre of the IIC SAS, TnUAD, FChPT STU and FunGlass, Študentská 2, 911 50 Trenčín, Slovakia

(E-mail: monika.michalkova@tnuni.sk)

<sup>2</sup> FunGlass, A. Dubček University of Trenčín, Študentská 2, 911 50 Trenčín, Slovakia

<sup>3</sup> CEITEC BUT, Brno University of Technology, Purkynova 123, Brno, Czech Republic

### ABSTRACT

The work deals with the preparation of bulk glass with yttrium aluminium garnet (YAG) composition from glass microspheres prepared by flame synthesis. Viscous flow sintering of the microspheres was performed to prepare bulk glass in a SPS. Dense translucent YAG glass were successfully prepared at temperatures below 950°C without isothermal heating.

Glass microspheres with YAG composition were prepared according to process described elsewhere [1]. Dense YAG glass and glass/ceramic samples were prepared by SPS (spark plasma sintering technique Dr Sinter SPS-625 from Fuji Electronic Industrial CO., LTD.). Carbon foil (0.5 mm thick) cladged graphite dies were filled with prepared YAG glass microspheres and sintered under vacuum at different conditions (see Tab. 1).

Table 1.: Summary of SPS sintering conditions and dilatation of the samples.

Sample	Pressure [MPa]	Heating rate [°C/min]	Dilatation of sample [mm]	max T [°C]
SPS 921	60	50	1.91	902.1
SPS 922	70	50	2.02	898.9
SPS 924	80	50	2.28	904.1

The density of sintered samples was measured by Archimedes' method in water.

The phase composition of sintered samples was determined by X-ray powder diffraction (XRD) using a Panalytical Empyrean DY1098 diffractometer, operated at 40 kV and 45 mA with Cu K $\alpha$  radiation ( $\lambda = 0.15405$  nm). The data were acquired over a  $2\theta$  range of 10-80° (step size 0.01 °, 50 s/step). The data were evaluated using the High Score Plus software with the crystallographic open database (COD 2018).

The XRD analysis of SPS sintered samples at different uniaxial pressures (60, 70 and 80 MPa) revealed that all samples are XRD amorphous. Hence, the densification temperature was set below the onset of the crystallization temperature. The shrinkage of the samples mentioned in Tab. 1 together with XRD analysis leads towards the conclusion that the densification was successfully done by viscous-flow sintering.

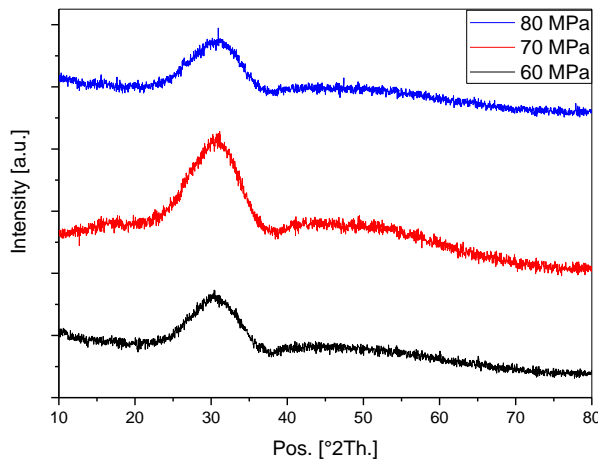


Fig. 1. XRD patterns of glasses with YAG composition SPS densified at different pressures.

Additionally, Fig. 2 presents the photography of prepared translucent YAG glass/ceramic samples with diameter of 12 mm placed directly on the text. The translucency was achieved in two cases: (a) at the pressure of 60 MPa and temperature 902 °C and (c) 80 MPa and temperature 904 °C. Opacity in the sample shown in Fig. 2 (b) was ascribed to the lower densification temperature 899 °C compare to the 902 °C used in the (a) case despite of the fact that higher pressure of 70 MPa to the 60 MPa between the (b) and (a) trials, was applied.



Fig. 2: The photograph of the prepared translucent YAG glass/ceramic with diameter 12 mm placed on the text. Pressure used during densification a) 60 MPa; b) 70 MPa; c) 80 MPa.

This work describes successful preparation of translucent glass with YAG composition at temperatures below 950 °C without dopants widening the kinetic window. Lower temperature leads to opaque white sample while increasing of the densification temperature resulted in translucent samples.

**Keywords:** flame synthesis, microspheres, SPS, YAG

**Acknowledgment:**



This item is a part of dissemination activities of project [FunGlass](#). This project has received funding from the European Union's Horizon 2020 research and innovation programme under grant agreement No 739566.

**References:**

[1] Chovanec, J.; Svoboda, R.; Kraxner, J.; Černá, A.; Galusek, D. Crystallization kinetics of the  $Y_3Al_5O_{12}$  glass. *Journal of Alloys and Compounds* 725 [25] (2017), pp. 792-799.

## Synthesis and sintering of nanocrystalline Ce<sup>3+</sup> - doped yttria nanoparticles prepared by precipitation method

**Nibu Putenpurayil Govindan<sup>1</sup>, Monika Micháľková<sup>2</sup>, Peter Švančárek<sup>2</sup>, Róbert Klement<sup>1</sup>  
Dušan Galusek<sup>1,2</sup>,**

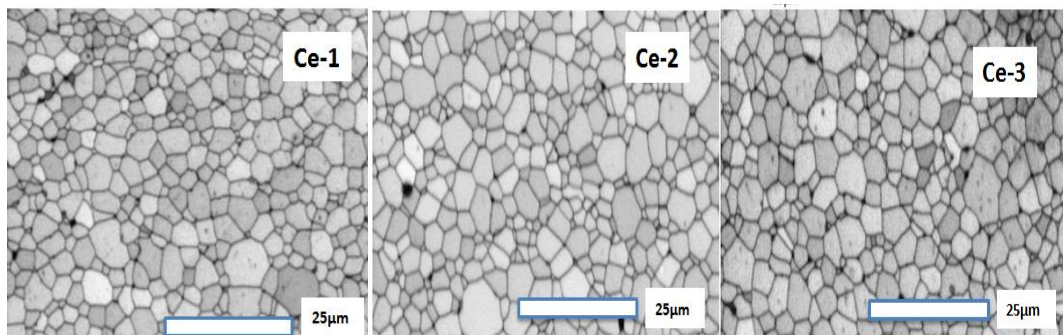
<sup>1</sup> – FunGlass - Centre for functional and surface functionalized glass, TnUAD, Trenčín, Slovakia  
(E-mail:nibu.puthenpurayil@tuni.sk)

<sup>2</sup> - Vitrum Laugaricio – Joint Glass Center of the IIC SAS, TnU AD, and FChPT STU, Trenčín, Slovakia,

Cubic yttria is widely known as a promising optical material owing to its broad range transparency, outstanding refractoriness, and excellent chemical stability. Using nanoparticle as starting material is found to be potential to fabricate ceramics not only achieving transparency but also considerably diminish sintering temperature [1, 2].

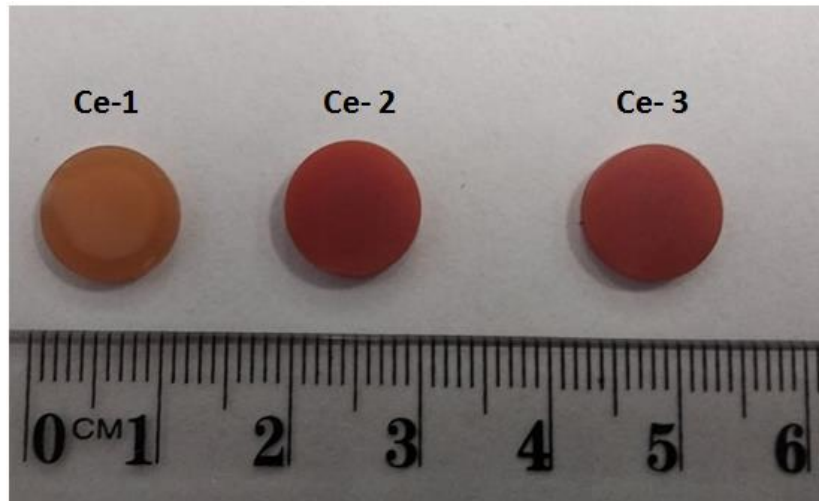
Cerium doped yttrium oxide ( $Y_{1.999}Ce_{0.001}O_3$ ,  $Y_{1.995}Ce_{0.005}O_3$ ,  $Y_{1.99}Ce_{0.01}O_3$ ) nanoparticles have been synthesized by precipitation method. The vacuum - pressure filtration was performed in a special die with a diameter of 15 mm. The suspension (30 vol % solid loading) was poured into the die and after losing the mould, a pressure of 20 bars was applied by a hydraulic press. The water from the suspension was drained through massive perforated metal bottom with a polymeric membrane (pore size 0.2  $\mu\text{m}$ ). The green body was air-calcined at 900 °C to remove the organic and then sintered at 1550 °C for 3 hrs at a heating rate of 10 °C/min. The samples were hot isostatic pressing (HIP) at 1500 °C for 1 h under an Ar gas pressure of 180 MPa. Relative density of sintered samples was determined by Archimedes principle in water.

Figure 1 shows the EBSD image of polished ceria doped yttria ceramics prepared by vacuum pressure filtration, sintered at 1550 °C for 3 hrs. The samples are coarse-crystalline with compact grain structure, sintered to high density, with closed porosity. The grain boundaries were sharply defined and grains are in range 2-6  $\mu\text{m}$ . Ceria doping did not show any influence on the microstructure of the sintered ceramics.



**Fig. 1:** The EBSD image of sintered samples and particle size distribution Ce<sup>3+</sup> doped Y<sub>2</sub>O<sub>3</sub> ceramics, Ce-1) 0.001 mol % Ce<sup>3+</sup>, Ce-2) 0.005 mol % Ce<sup>3+</sup>, Ce-3) 0.01 mol % Ce<sup>3+</sup>.

Figure 2 shows the image of polished ceria doped yttria ceramics after applying the hot isostatic press (HIP, 1500 °C for 1 h). The samples show an orange-reddish colour which is due to the doping of the samples with Ce<sup>3+</sup>. Consequently, doping of sample with 0.001 mol % Ce<sup>3+</sup> resulted in light orange colour, while increasing of the dopant concentration leads to the darker orange-reddish colour. It is caused by the presence of oxygen vacancies resulted from the reducing conditions in the HIP, which give rise to the formation of F and F<sup>+</sup> centers in the wide band gap [3, 4].



**Fig. 2:** Photography of ceria doped yttria ceramics hot isostatic pressing (HIP) at 1500 °C for 1 h, Ce-1) 0.001 mol % Ce<sup>3+</sup>, Ce-2) 0.005 mol % Ce<sup>3+</sup> Ce-3) 0.01 mol % Ce<sup>3+</sup>.

The relative density of Ce<sup>3+</sup> doped yttria ceramics before and after HIP is summarized in Table 1. Generally, increasing of the dopant concentration leads to the higher densities after sintering. This is more obvious before applying HIP, where the difference in density between 0,001 Ce<sup>3+</sup> and 0, 01 Ce<sup>3+</sup> is almost 0.7 %.

**Table 1:** Relative density of Ce<sup>3+</sup> doped yttria ceramic.

Sample	Relative density	
	1550 °C /3h	HIP 1500°C /1h
0.001 Ce <sup>3+</sup>	97.88 %	99.75%
0.005 Ce <sup>3+</sup>	98.38 %	99.79%
0.010 Ce <sup>3+</sup>	98.57 %	99.89%

**Keywords:** Ceramic, EBSD, HIP, Precipitation, Y<sub>2</sub>O<sub>3</sub>.

**Acknowledgment:**



This paper is a part of dissemination activities of VEGA 2/0026/17, SAS-MOST 2015-06 and FunGlass. This project has received funding from the European Union's Horizon 2020 research and innovation programme under grant agreement No 739566.

**References:**

- [1] X. Song, *Journal of Rare Earths*. 29, 155–159. (2011)
- [2] R. V, Mangalaraja, *Powder Technology*. 191, 309–314.(2009)
- [3] A. Krell, *Optical Materials* 31, 1144–1150. (2009)
- [4] I.S, Zhukov, *Mendeleev Commun*. 29, 102–104. (2019)

## Chemical Tempering of Flexible Glasses

Ali Talimian<sup>1</sup>

<sup>1</sup> Centre for Functional and Surface Functionalised Glass, Alexander Dubcek University of Trencin, Trencin, Slovakia  
(E-mail: ali.talimian@unitn.sk)

### ABSTRACT

Since last decade, smartphones have revolutionised human life; however, this market, which was booming a couple of years ago, has driven into stagnation due to lacking materials able to cope with the demand for better, smaller and stretchable devices. This bottleneck can be overcome by using chemically tempered glasses that are strong and flexible despite being brittle.

This presentation explores the chemical tempering of thin silicate glasses; influences of being subjected to Na-K ion exchange and typical parameters, such as temperature and time, on the generation of compressive residual stress and mechanical properties have been investigated.

**Keywords:** Chemical tempering, Silicate Glass, Mechanical properties.

### Acknowledgment:



This item is a part of dissemination activities of project [FunGlass](#).  
This project has received funding from the European Union's Horizon 2020 research and innovation programme under grant agreement No 739566.

## Study of thermal behavior and PL properties of $\text{Yb}_2\text{O}_3\text{-Al}_2\text{O}_3$ glass microspheres

**J. Valúchová<sup>1,2</sup>, A. Prnová<sup>1,2</sup>, A. Plško<sup>2</sup>, R. Klement<sup>2</sup>, M. Majerová<sup>3</sup>, D. Galusek<sup>1,2</sup>**

<sup>1</sup>*Institute of Inorganic Chemistry of Slovak Academy of Sciences, Bratislava, Dúbravská cesta 9, SK-845 36, Slovakia*

<sup>2</sup>*VILA – Joined Glass Centre of the IIC SAS, TnUAD, FChPT STU, Študentská 2, SK-911 50 Trenčín, Slovakia*

<sup>3</sup>*Department of Magnetometry, Institute of Measurement Science, Slovak Academy of Sciences, Dúbravská cesta 9, 841 04 Bratislava, Slovak Republic*

The ytterbium aluminium garnet composition ( $\text{Yb}_3\text{Al}_5\text{O}_{12}$ ), YbA-G (62.5 mol.%  $\text{Al}_2\text{O}_3$ , 37.5 mol.%  $\text{Yb}_2\text{O}_3$ ), was prepared in the form of glass microspheres by flame synthesis, using a methane-oxygen flame. To obtain a high homogeneity of glass microspheres, a modified sol-gel Pechini method [1] was used to prepare the starting powder. Only the presence of a wider hump in the interval  $23\text{-}40^\circ$  in 2-theta range was observed in the XRD pattern of the prepared glass microspheres, which indicates the predominantly amorphous nature of the sample. However, the next detailed study on the morphology of the prepared system by scanning electron microscopy (SEM) showed the presence of a small portion of partially, or fully, crystallised microspheres (Fig. 1). The high-temperature X-ray powder diffraction analysis (HT XRD) was carried out in the temperature interval of  $750\text{-}1450^\circ\text{C}$ , and with a step size of  $5^\circ\text{C}$ , to determine the temperature influence on the phase composition. Only the crystallisation of  $\text{Yb}_3\text{Al}_5\text{O}_{12}$ , a ytterbium aluminium garnet phase (COD-04-001-9735), was observed throughout the temperature range. The DSC analyses, with heating rates of 2, 4, 6, 8, and  $10^\circ\text{C}/\text{min}$ , in the temperature interval of  $25\text{-}1200^\circ\text{C}$ , were performed in a  $\text{N}_2$  atmosphere to better understand the temperature behaviour of the prepared glass microspheres. Two exothermic effects at  $910^\circ\text{C}$  and  $933^\circ\text{C}$  were observed, which can be attributed to the crystallisation of  $\text{Yb}_3\text{Al}_5\text{O}_{12}$ . The crystallization kinetics of the prepared sample were examined in terms of the JMAK model and the kinetic triplet (frequency factor  $A$ , apparent activation energy  $E_{\text{app}}$ , and the Avrami coefficient  $m$ ) was determined (Tab. 1) using RSS,  $R^2_{\text{adj}}$ , and AIC criteria. Finally, the PL spectra was measured and results were compared with results of our previous work and discussed.

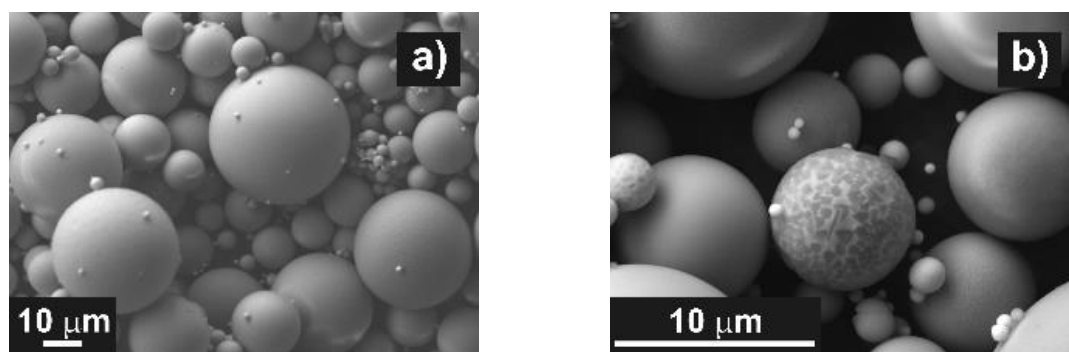


Fig. 1 SEM analysis a) prepared YbA-G sample, b) detail of crystallized microsphere

Tab. 1 The determined kinetic triplets

Peak	$m$	$A \pm \text{sd}$ [ $\text{min}^{-1}$ ]	$E_{\text{app}} \pm \text{sd}$ [ $\text{kJ}\cdot\text{mol}^{-1}$ ]
1	3	$(1.76 \pm 2.0)10^{28}$	$(6.39 \pm 0.08)10^5$
2	2	$(1.28 \pm 1.6)10^{55}$	$(1.27 \pm 0.09)10^6$

## Acknowledgment



This paper is a part of dissemination activities of project FunGlass. This project has received funding from the European Union's Horizon 2020, research and innovation programme under grant agreement No 739566. The financial support of this work by the projects APVV 0014-15, APVV 0049-17, VEGA 1/0527/18, VEGA 2/0026/17, VEGA 2/0088/16, VEGA 1/0064/18 is gratefully acknowledged.

## References

- [1] M. P. Pechini, "Method of Preparing Lead and Alkaline-Earth Titanates and Niobates and Coating Method Using the Same to Form a Capacitor," U.S. Pat. No. 3330697, July 11, 1967
- [2] A. Prnová, K. Bodišová, R. Klement, M. Migát, P. Veteška, M. Škrátek, E. Bruneel, I. Van Driessche, D. Galusek, Preparation and characterization of  $\text{Yb}_2\text{O}_3 - \text{Al}_2\text{O}_3$  glasses by the Pechini sol – gel method combined with flame synthesis, 40 (2014) 6179–6184. doi:10.1016/j.ceramint.2013.11.071.

# Structure and properties analysis by the Associate Solutions Thermodynamic Model in BaO-P<sub>2</sub>O<sub>5</sub> glasses

**Rajesh Dagupati<sup>1</sup>, Alberto Lopez<sup>2</sup>, Marek Liška<sup>1</sup>, Francisco Munoz<sup>2</sup>**

<sup>1</sup> Centre for Functional and Surface Functionalized Glass, Alexander Dubček University of Trenčín  
(E-mail: [rajesh.dagupati@tuni.sk](mailto:rajesh.dagupati@tuni.sk), [marek.liska@tuni.sk](mailto:marek.liska@tuni.sk))

<sup>2</sup> Institute of Ceramics and Glass (CSIC), Kelsen 5, 28049 Madrid, Spain  
(E-mail: [fmunoz@icv.csic.es](mailto:fmunoz@icv.csic.es))

## ABSTRACT

Disclosing of composition-structure-property relationship in various glasses either by experimental techniques and/or theoretical models has significant research in the glass science since couple of decades. Rather than studying using highly sophisticated experimental tools, such as solid-state nuclear magnetic resonance (NMR) spectroscopy, X-ray absorption spectroscopy (XAS), and neutron diffraction analysis etc., the thermodynamic model of associate solutions (SVTDM) has grab our attention to study the structure of the glasses, especially phosphate glasses. This model was developed in glasses by Shakhmatkin and Vedishcheva [1], and applied to silicate, borate, phosphate and chalcogenide glasses to predict their structure. Moreover, the model applicability has been verified by comparing the predicted structure with the structure studied experimentally and predicted physical parameters value with measured value.

As we knew that, phosphate glasses possess remarkable functional properties such as low viscosity, high refractive indices, lower melting temperature as compared to silicate and borate glasses, high thermal expansion coefficient and the high transparency in the ultraviolet range which make them excellent candidates for glass to metal sealing applications, vitrification of radioactive waste and photonics [2, 3]. So that studying the structure of binary barium phosphate glasses through the SVTD model has worthwhile.

The main objective of this work is that study the structure of BaO-P<sub>2</sub>O<sub>5</sub> glasses through the SVTD model and verification of its applicability by study the structure experimentally through the MAS-NMR analysis. Furthermore, the physical and thermodynamic properties of the glasses against BaO content will be evaluated.

In order to study the structure experimentally glass samples with chemical composition (100-x) P<sub>2</sub>O<sub>5</sub>-x BaO, where x = 40, 42.5, 45, 47.5, 50, 52.5, 55, and 57.5 mol% were prepared using melt and quenching technique. These glasses hereafter labeled as 40\_BaO, 42.5\_BaO, 45\_BaO, 47.5\_BaO, 50\_BaO, 52.5\_BaO, 55\_BaO and 57.5\_BaO for the respective 40, 42.5, 45, 47.5, 50, 52.5, 55 and 57.5 mol% of BaO content.

## SVTD Model for BaO-P<sub>2</sub>O<sub>5</sub> glasses

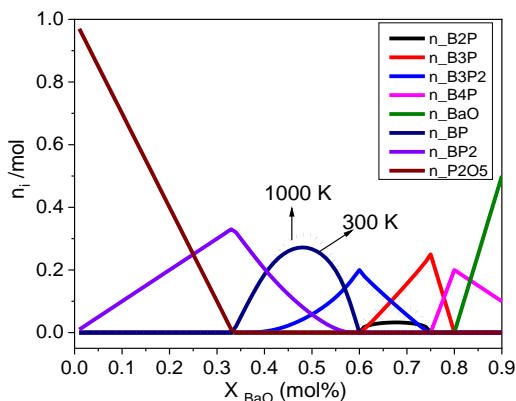


Fig. 1

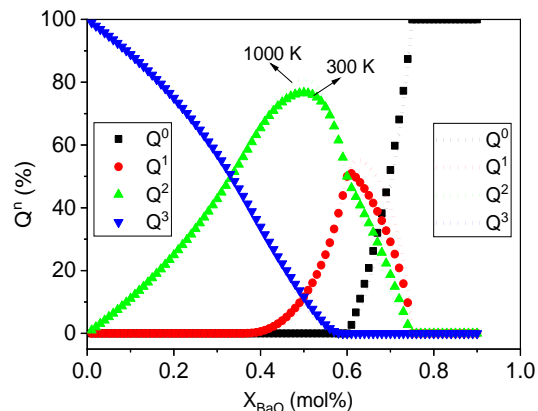


Fig. 2

In order to construct the thermodynamic model, we computed equilibrium molar amounts and molar fractions of the input components (stable crystalline components that have identified through the phase diagram [4] and systems components) from corresponding Gibbs energies taken from the FACT data base (except B3P2 phase) at different temperatures, 300 and 1000 K. The equilibrium molar amounts of input components against BaO content represents the SVTD model, depicted in Fig. 1 for BaO-P<sub>2</sub>O<sub>5</sub> glasses. Two pseudo-regions i.e. (i), binary ( $0 \leq x \leq 0.33$ ) and (ii) ternary ( $0.33 \leq x \leq 0.60$ ) regions have been observed in the glass forming region ( $< 60$  mol% BaO). The tetrahedral units Q<sup>n</sup> (n= 0, 1, 2, and 3) that are presented in the glasses were calculated based on equilibrium molar fraction of the input components and their variation against BaO content illustrated in Fig. 2. For selected glasses, theoretical and analyzed composition and predicted tetrahedral units Q<sup>3</sup>, Q<sup>2</sup> and Q<sup>1</sup> from the model and the MAS-NMR analysis are tabulated in the following table 1. Furthermore, the molar volume (V<sub>M</sub>) of the investigated glasses was predicted through the model based on the molar volume of input components and has coincide with the measured value with maximum error ( $\leq 6$  %).

**Table 1:** Theoretical and analyzed compositions in mol%, and Q<sup>n</sup> (n= 0, 1, 2, and 3) tetrahedral units obtained from the model and MAS-NMR analysis against BaO content for selected glasses.

Glass	Theoretical		Analyzed			SVTD Model (in %)			MAS-NMR (in %)		
	P <sub>2</sub> O <sub>5</sub>	BaO	P <sub>2</sub> O <sub>5</sub>	BaO	Al <sub>2</sub> O <sub>3</sub>	Q <sup>3</sup>	Q <sup>2</sup>	Q <sup>1</sup>	Q <sup>3</sup>	Q <sup>2</sup>	Q <sup>1</sup>
42.5_BaO	57.5	42.5	56.42	41.53	2.05	27	72	1	21	79	0
45_BaO	55.0	45.0	54.57	44.17	1.23	21	76	3	17	83	0
50_BaO	50.0	50.0	49.87	48.85	1.24	10	80	10	10	84	6
52.5_BaO	47.5	52.5	47.13	51.84	1.40	5	79	16	5	72	23
55_BaO	45.0	55.0	45.87	53.40	0.72	2	74	24	0	72	28

**Keywords:** Barium Phosphate glasses; SVTD Model; Structure; MAS-NMR; Viscosity of liquid flow;

#### Acknowledgment:



This item is a part of dissemination activities of project [FunGlass](#). This project has received funding from the European Union's Horizon 2020 research and innovation programme under grant agreement No 739566.

#### References:

- [1] B. A. Shakhmatkin, N. M. Vedishcheva and A. C. Wright, *Non-Cryst. Solids* 293-295 (2001) 220-226.
- [2] K. Suzuya, D. L. Price, C.K. Loong, and S.W. Martin, *J. Non-Cryst. Solids*, 232–234, (1998) 650–657.
- [3] R.K. Brow, and D.R. Tallant, *J. Non-Cryst. Solids*, 222 (1997) 396–406.
- [4] R. A. McCauley and F. A. Hummel, *Trans. Br. Ceram. Soc.*, 67 [12] (1968) 619-628.

## Network Mediated Coupling in Phosphate Glasses

**K. Griebenow<sup>1</sup>, E.I. Kamitsos<sup>2</sup>, L. Wondraczek<sup>1,3</sup>**

<sup>1</sup>Otto Schott Institute of Materials Research, University of Jena, Germany

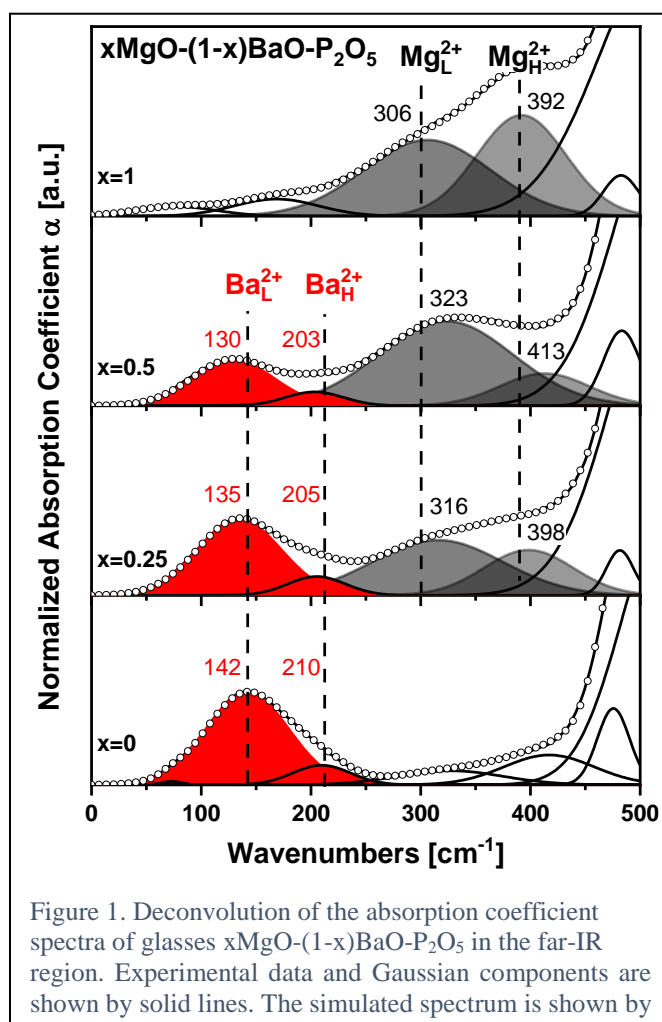
(E-mail: kristin.griebenow@uni-jena.de)

<sup>2</sup>Theoretical & Physical Chemistry Institute, National Hellenic Research Foundation, Athens, Greece

<sup>3</sup>Abbe Center of Photons, Jena, Germany

### ABSTRACT

Mixed Mg-Ba metaphosphate (MP) glasses with the nominal composition  $x\text{MgO}-(1-x)\text{BaO}-\text{P}_2\text{O}_5$   $x=0, 0.25, 0.5, 0.75, 1.0$  were prepared by conventional melt-quench technique. The glasses were investigated by vacuum FTIR spectroscopy in order to characterize the specific cation-oxygen bonds (for detailed information see Ref. 1).



Ba-O vibration frequency decreases from 142 to 130  $\text{cm}^{-1}$  as Mg ions are introduced. This suggests a corresponding weakening of the Ba-O interaction. The relative population of Mg in octahedral sites increases upon cation mixing and the Mg-O interactions become stronger in both octahedral and tetrahedral sites.

These results provide evidence for mixing of Mg and Ba at the atomic scale, i.e. for the formation of Ba-O-Mg configurations where polarization effects through the shared oxygen ions influence the Ba-O and Mg-O bond in the opposite way.

The far-infrared ( $<400 \text{ cm}^{-1}$ ) region provides information on the metal-oxygen motions, i.e. the rattling of the cations against their oxygen cage. The cage rattling can be roughly approximated as harmonic oscillation of the cation within a symmetric oxygen environment.

The far-IR spectra of the Mg-Ba MP glasses and their deconvolution into Gaussian components are shown in Figure 1. The pure Mg MP glass ( $x=1$ ) shows two bands at 306 and 392  $\text{cm}^{-1}$  which are assigned to Mg-O stretching vibrations in octahedral low-basicity sites ( $\text{MgO}_6$ ) and tetrahedral high-basicity sites ( $\text{MgO}_4$ ) respectively<sup>2,3</sup>.

The Ba-O stretching in the pure Ba MP glass is measured at 142  $\text{cm}^{-1}$  (low-basicity) and 210  $\text{cm}^{-1}$  (high-basicity)<sup>4</sup>. Besides the strong M-O stretching modes, minor features are found at 170 (see pure Mg MP spectra), 333 and 418  $\text{cm}^{-1}$ . These latter are attributed to rotations of  $\text{PO}_4$  tetrahedra and deformations of phosphate units<sup>2,5</sup>.

Mixing Mg and Ba ions in one glassy network leads to systematic variations in the cation-oxygen motion bands. The

Far-IR spectroscopy shows that in mixed cation MP glasses the M-O interactions strengthen (weaken) for the high-field strength (low field strength) ion as a result of mixing.

**Keywords:** FTIR, glass, modifier effect, phosphate, structure

**Acknowledgment:**



This item is a part of dissemination activities of project [FunGlass](#).  
This project has received funding from the European Union's Horizon 2020 research and innovation programme under grant agreement No 739566.

**References:**

- <sup>1</sup> K. Griebenow, C.B. Bragatto, E.I. Kamitsos, L. Wondraczek, J. Non-Cryst. Solids 481 (2018) 447-456
- <sup>2</sup> K. Griebenow, E.I. Kamitsos, L. Wondraczek, J. Non-Cryst. Solids 468 (2017) 74-81
- <sup>3</sup> B.N. Nelson, J. Gregory Exarhos, J. Chem. Phys. 71 (1979) 2739-2747
- <sup>4</sup> L.L. Velli, C.P.E. Varsamis, E.I. Kamitsos, D. Moencke, D. Ehrt, Phys. Chem. Glasses 46 (2005) 178-181
- <sup>5</sup> I. Konidakis, C.P.E. Varsamis, E.I. Kamitsos, D. Moencke, D. Ehrt, J. Phys. Chem. C 1147 (2010) 9125-9138

## Effect of nucleating agents on the characterization of basaltic glass ceramics

**M.A. Mahmoud<sup>1, 2</sup>, G.A. Khater<sup>2</sup>, M.R. Shehata<sup>3</sup> and J. Kraxner<sup>1</sup>**

<sup>1</sup> Glass Processing Department, FunGlass, Alexander Dubček University of Trenčín, Slovak Republic  
(E-mail: mokhtar.mahmoud@tnuni.sk)

<sup>2</sup> Glass Research Department, National Research Centre, Cairo, Egypt

<sup>3</sup> Chemistry Department, Faculty of Science, Cairo University, Egypt

### ABSTRACT

Basaltic glass ceramics were prepared successfully based on basalt rocks with successive addition of cement wastes from 10-50 % of the batch constituents, six glass batches are designated G0, G10, G20, G30, G40 and G50, where the number indicates to the weight percent added of the cement waste and the rest is the basaltic rocks. Basaltic rocks were crushed and sieved into 75  $\mu\text{m}$  before mixing with cement waste, the corresponding batches were generally melted in platinum crucibles at 1400 °C for 2h, the melt cast into a steel plate in the form of discs and rods shapes, then transferred to a preheated muffle furnace at 550 °C, which then switched off to cool at room temperature to prevent rupturing the samples, then glass samples subjected to heat treatments at 1000 °C for 2h to induce crystallization and to convert glass into glass ceramics. XRD showed major crystalline phases were Diopside, Anorthite, Gehlenite and Magnetite. SEM showed the microstructure gradually changed from very fine grain into coarse grain microstructure by increasing cement waste ratio, unfortunately the coarse grain microstructure provided a negative effect on the mechanical properties of the obtained glass ceramics, where the microhardness and the bending strength decreased sharply from 6791 to 4077 MPa and from 135 to 77 MPa respectively [1, 2].

For this reason, we studied the effect of some nucleating agents on the microstructure of the obtained glass ceramics which in turn could improve the mechanical properties of the resultant materials. The batch G30 (70% basalt + 30% cement waste) was chosen for study the role of some selected nucleating agents such as  $\text{Cr}_2\text{O}_3$ ,  $\text{ZrO}_2$  and  $\text{CaF}_2$ , the nucleating agents added to the batch G30 with two different weight ratios as shown 1 and 2 % for  $\text{Cr}_2\text{O}_3$  and  $\text{ZrO}_2$ , and 2 and 4 % for  $\text{CaF}_2$ . Six nucleated glass batches are designated G 1Cr, G 2Cr, G 1Zr, G 2Zr, G 2Ca, and G 4Ca, where the numbers indicate the weight ratio added for each selected nucleating agents. Nucleated glass batches melted at 1350-1400 °C according to the batch composition, and then the obtained glass samples subjected to heat treatment at 1000 °C for 2 h to induce the crystallization process.

DTA showed presence of  $\text{Cr}_2\text{O}_3$  increased the exothermic crystallization peak from 883°C for G30 (nucleating agents free) into 895 °C and 903 °C for G 1Cr and G 2Cr respectively, and regard to addition of  $\text{ZrO}_2$ , it's noticed practically increase the viscosity of the produced melts as compared to the basic glass sample (G30) and exothermic temperature reached 910 and 915 °C for G 1Zr and G 2Zr respectively, unlike  $\text{CaF}_2$ , It reduced melting temperature as well as the viscosity of the produced melt, also the crystallization exothermic peak decreased to 870, 845°C for G 2Ca and G 4Ca glasses respectively. XRD showed presence of nucleating agents in glass G30 generally facilitates and favors the formation of wollastonite ( $\text{CaSiO}_3$ ), quartz ( $\text{SiO}_2$ ), stabilize formation of diopside ( $\text{CaMgSi}_2\text{O}_6$ ), anorthite ( $\text{CaAl}_2\text{Si}_2\text{O}_8$ ) and magnetite ( $\text{Fe}_3\text{O}_4$ ) [3].

From Fig.1 SEM micrograph, glass ceramics containing  $\text{Cr}_2\text{O}_3$  showed unsimilar fabrics to the base G30 (nucleating agents free), although both are consisting of ribbon structure of diopside- anorthite, where it showed homogenous fine grained crystals, the average of the crystals sizes of G 2Cr and G 1Cr are 50 nm and 150 nm respectively, while the average crystals size of the base glass ceramic (G30) is 7 $\mu\text{m}$ . The shapes of the crystals of both G 1Cr and G 2Cr are very minute and similar to each other, therefore  $\text{Cr}_2\text{O}_3$  effectively motivated development uniform bulk crystallization of particularly fine-grained microstructures, while glass ceramics containing  $\text{ZrO}_2$  showed rigid cubic crystals with a great number of crystallization centers, the average of crystals sizes of G 1Zr and G 2Zr are 6  $\mu\text{m}$  and 1  $\mu\text{m}$  respectively, whereas glass ceramics containing  $\text{CaF}_2$  showed effectively formation of large non-

uniform texture of extremely coarse-grained microstructures which is larger than the base glass ceramic sample, the shapes of the crystals of both of G 2Ca and G 4Ca are fiber and needles shapes, the average crystal size of G 2Ca and G 4Ca is ranging from 50 -150  $\mu\text{m}$ .

According to the mechanical measurements, the nucleated glass ceramic samples have higher microhardness and bending strength values than the base glass ceramics except for  $\text{CaF}_2$  nucleated glass ceramics. Sample G 2Cr has the highest microhardness value (5885 MPa), while the corresponding base sample G30 was (4841 MPa) and that reflected the efficacy of  $\text{Cr}_2\text{O}_3$  nucleating agent for enhancement the microstructure as well as improvement the strength, whereas G 4Ca has the lowest microhardness value (4835 MPa), while samples contained  $\text{ZrO}_2$  showed middle effect of microhardness as shown 5400 and 5120 MPa for G 1Zr and G 2Zr respectively. Also it was found that G 2Cr has the highest value of bending strength (141 MPa) and that confirmed how  $\text{Cr}_2\text{O}_3$  has a great role for initiating homogeneous crystallization which in turn increased the degree of strength, while  $\text{ZrO}_2$  has a middle effect on bending strength measurements (95 MPa), G 4Ca has the lowest bending strength value (81 MPa), while bending strength for the base glass ceramic is 88 MPa [3].

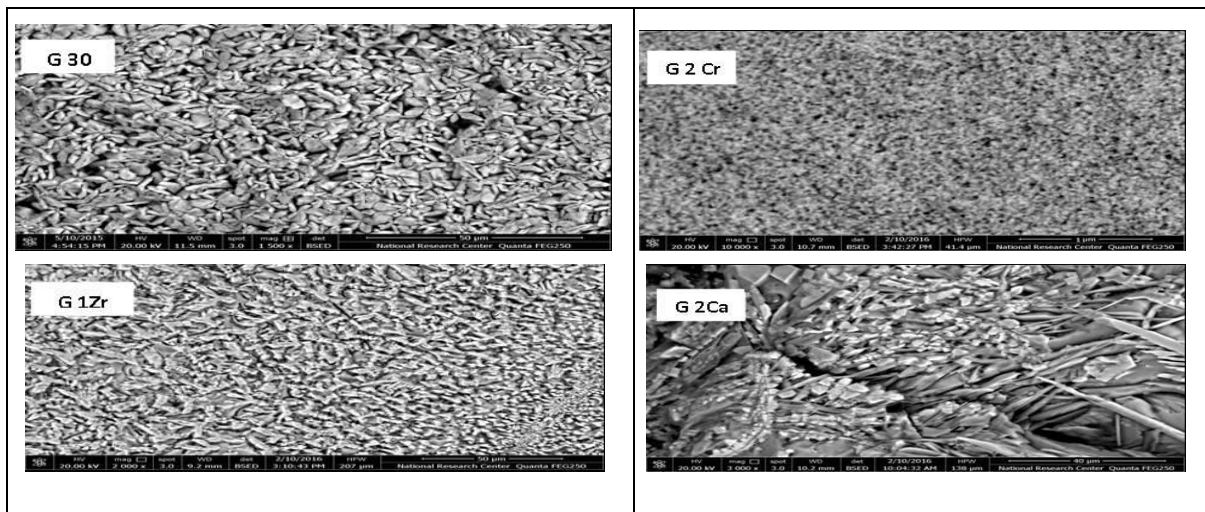


Fig.1 SEM micrographs of the base and nucleated glass ceramics

**Keywords:** Basalt, Cement Waste, Crystallization, Glass Ceramics, Nucleating Agents

**Acknowledgment:**



This item is a part of dissemination activities of project [FunGlass](#). This project has received funding from the European Union's Horizon 2020 research and innovation programme under grant agreement No 739566.

**References:**

- 1- G.A. Khater, M.R. Shehata, E.M.A. Hamzawy and **M.A. Mahmoud** "Preparation of glass-ceramic materials from basaltic rocks and by-pass cement dust" *Glass Technology: European Journal of Glass Science and Technology Part A*, 58 (1) (2017) p.17-25.
- 2- G. A. Khater, Yunlong Yue, M. O. Abu Safiah and **M. A. Mahmoud** "Synthesis and characterization of anorthite and magnetite glass-ceramics from basaltic rocks" *Silicon Journal*, 11(4) (2018) p.1763-1774.
- 3- G.A. Khater and **M.A. Mahmoud** "Preparation and characterization of nucleated glass-ceramics based on basaltic rocks" *Journal of the Australian Ceramic Society*, 52(8) (2017) p.1-9.

## **Fundamentals of solid state Nuclear Magnetic Resonance and application to the structure of glasses**

**Francisco Muñoz**

Institute of Ceramics and Glass (CSIC), Kelsen 5, 28049 Madrid (Spain)  
(E-mail: fmunoz@icv.csic.es)

### **ABSTRACT**

Glasses are homogeneous and isotropic solids that result from the rapid cooling from their respective melts and that possess a transition between the liquid and rigid states that occurs in a continuous and reversible fashion without phase change at the so-called glass transition temperature. Some of the most common properties of glasses constitute the group of additive properties, which can be tuned through adequate modifications of the composition, thus being expressed by a linear combination of the molar fractions of the constituting oxides. On the other hand, and despite glasses present a short range structural order without periodicity, there are compositionally dependent structural arrangements that give rise to non-linear variations of certain other properties that involve charge or mass displacement throughout the glass network. The last can be the chemical, electrical or rheological properties, all belonging to the group of the transport properties of glass. Two well-known examples of the last are responsible for the mixed-alkali effect or boron anomaly.

Nuclear Magnetic Resonance is nowadays one of the most powerful techniques to accomplish the difficult task of properly determining the structure of glasses. Selectivity is one of the great advantages of magnetic resonance methods, which contributes to make NMR a very versatile analytical tool in the study of glasses. Furthermore, by combining all different interactions upon the magnetic field influence, one may obtain information on coordination numbers, distances and bonding angles and on the geometry of the structural groupings that constitute the network. The use of higher magnetic fields and the numerous specific multi-nuclear correlation sequences have also considerably improved the resolution of the NMR spectra in solids and amorphous materials in particular, allowing for an exceptional accuracy in the determination of glass structure.

The talk will be divided into two sections; the first being devoted to the fundamentals of NMR spectroscopy from the point of view of the solid state through a brief review of the basics and most important methods on acquisition and simulation of spectra. Then, a concise analysis of the glassy state and the theories of glass structure will be presented, followed by an extensive list of examples on the application of solid state NMR in the elucidation of the structure of silicate, borate and phosphate based glasses, as the main glass forming oxides. The use of Nuclear Magnetic Resonance will show that it is not only possible to study the closest chemical environment of the active NMR nuclei under study but also that one may obtain information concerning the connectivity between adjacent structural groups and how these influence glass properties. The talk will also cover examples on advanced techniques such as REDOR (Rotational echo double resonance) or TRAPDOR (Transfer of population in double resonance), that are useful in the study of the positions of modifier cations and the bonding between the structural groupings forming the network, to finalize with the application of NMR in the study of anionic species, such as  $O^{2-}$ ,  $N^{3-}$  or  $F^-$ .

**Keywords:** Structure; Glasses; Nuclear Magnetic Resonance; Spectroscopy.

**Acknowledgment:** F.M. thanks funding for projects MAT2017-87035-C2-1-P, (AEI/FEDER, UE) and FUNGLASS from EC under grant agreement 739566.



This item is a part of dissemination activities of project [FunGlass](#).  
This project has received funding from the European Union's Horizon 2020 research and innovation programme under grant agreement No 739566.

**References:**

1. R.K. Brow, M.L. Schmitt, J. Eur. Ceram. Soc. 29 (2009) 1193.
2. J.M.F. Navarro, El Vidrio, Consejo Superior de Investigaciones Científicas, Madrid (2003).
3. D. Massiot, Spectra analyse 21(224) (2002) 27.
4. L. Wondraczek *et al.*, Adv. Mater. 23 (2011) 4578.
5. W. H. Zachariasen, J. Am. Chem. Soc. 54 (1932) 3841.
6. T. Gullion, *et al.*, J. Magn. Res. 81 (1989), 196.
7. C.P. Grey, *et al.*, J. Am. Chem. Soc., 117 (1995) 8232.

## Thermodynamic study of the structure and properties of $\text{Li}_2\text{O}-\text{P}_2\text{O}_5$ glasses

Alberto López, Francisco Muñoz

Institute of Ceramics and Glass (CSIC), Kelsen 5, 28049 Madrid (Spain)  
(E-mail: alberto.lopez@icv.csic.es)

### ABSTRACT

Lithium phosphate glasses have been noticed to have excellent transport properties and for this reason, these glasses have been the subject of important research by glass scientists. The enhancement of the transport properties is due to the depolymerization of the glass network as  $\text{Li}_2\text{O}$  is added, where diffusion of  $\text{Li}^+$  cations occurs by a thermally activated hopping mechanism between non-bridging oxygens (NBO).

Although these glasses cannot be directly used in technological applications due to their poor chemical durability, they can be used as a base material to obtain products of higher technological interest, such as LiPON thin-films for solid-state batteries [1-3].

In the present study, the ionic conductivity of the glasses in a theoretical way without using any adjustable parameters is calculated by using three theoretical models: the weak electrolyte model (WEM) [4-8], the Anderson and Stuart Model (A&SM) [9] and the Shakhmatkin and Vedishcheva Thermodynamic Model (SVTDM) [10].

The WEM can be used in glasses to predict their ionic conductivity as a function of the total charge carrier concentration,  $n$ , and the attempt frequency ( $\nu_0$ ) and distance ( $\lambda$ ) of the cation's jump during diffusion:

$$\sigma T = n \frac{e^2 \lambda^2 \nu_0}{6k_B} \exp\left(-\frac{E_a}{k_B T}\right)$$

where the constants  $e$  and  $k_B$  are the fundamental charge unit and the Boltzmann constant.

By using this model, an Arrhenius expression is obtained for the product  $\sigma T$ , whose activation energy can be predicted in its turn by using A&SM. The model assumes that the required energy to move a cation is the sum of two contributions: the one necessary to move the cation (electrostatic energy change) presupposing that there is no change in the glass structure, and the one which is required to produce a deformation in the glass structure so as to produce a hole large enough for the cation to pass. The necessary values of the thermodynamic properties to use the WEM can also be calculated by using the SVTDM, which has also been tested in the prediction of the thermodynamic properties measured in this study. SVTDM assumes that a glass is an ideal solution of the salt-like products formed from the reaction of the oxides and the unreacted oxides as well. Thus, all the thermodynamic properties of the glasses can be derived from the Gibbs free energy expression of an ideal solution:

$$G = \sum n_i g_i + RT \sum n_i \ln(x_i)$$

where the molar Gibbs free energy ( $g_i$ ) of each reaction product can be precisely estimated by simply using the expression of the one for the corresponding crystalline phase of the equilibrium phase diagram of the system, as the short range structural order is very similar.

The comparison between the values calculated from this model and the experimental ones shows that the thermodynamic properties can be well predicted by using SVTDM. However, for the calculation of the ionic conductivity, a theoretical model for the prediction of the dielectric constant of the glasses as a function of the composition will be needed in order to predict the activation energy through the A&SM.

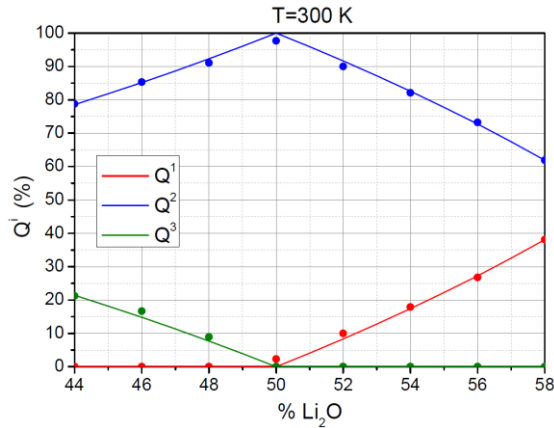


Figure 1: Q<sup>i</sup> structural groups: calculated (straight line) and experimental (dots).

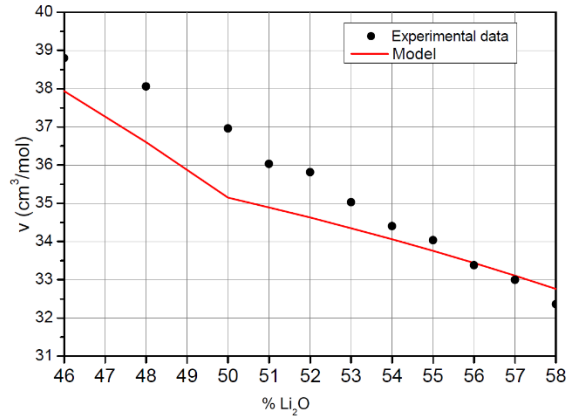


Figure 2: Molar volume of Li<sub>2</sub>O-P<sub>2</sub>O<sub>5</sub> glasses. T=300 K.



This item is a part of dissemination activities of project [FunGlass](#). This project has received funding from the European Union's Horizon 2020 research and innovation programme under grant agreement No 739566.

### References:

- [1] S. Nowak, F. Berkemier, G. Schmitz, J. Power Sources 275 (2015) pp. 144-150.
- [2] V. Lacivita, N. Artrith, G. Ceder, Chem. Mater. 2018, 30, 20, 7077-7090.
- [3] A. Sepúlveda, F. Criscuolo, B. Put, P.M. Vereecken, Solid State Ion. 337, pp. 24-32.
- [4] D. Ravaine, J.L. Souquet, Phys. Chem. Glasses 18 n°2 (1977) pp. 27-31.
- [5] D. Ravaine, J.L. Souquet, Phys. Chem. Glasses 19 n°5 (1978) pp. 115-120.
- [6] A. Kone, J.L. Souquet, Solid State Ion. 18-19 (1986), pp. 454-460.
- [7] J.L. Souquet, M. Levy and M. Duclot, Solid State Ion. 70/71 (1994) 337-345.
- [8] A.C. Martins Rodrigues, M.L. Ferreira Nascimento, C. Barca Bragatto, J.L. Souquet, J. Chem. Phys. 135, 234504 (2011).
- [9] O.L. Anderson, D.A. Stuart, J. Am. Ceram. Soc. 37(12) 573-580.
- [10] Shakhmatkin and Vedishcheva, Glass physics and chemistry 24(3) (1998) pp. 229-236.

## Spectral properties of inorganic-organic films on glass

**Alfonz Plško<sup>1</sup>, Katarína Faturíková<sup>1</sup>, Jana Pagáčová<sup>2</sup>, Iveta Papučová<sup>2</sup>,  
Mariana Švančárková<sup>1</sup>**

<sup>1</sup> FunGlass, Alexander Dubček University of Trenčín, Študentská 2,  
SK-911 50 Trenčín, Slovakia

<sup>2</sup> Faculty of Industrial Technologies in Púchov, Alexander Dubček University of Trenčín, I. Krasku 491/30,  
SK-020 01 Púchov, Slovakia

### ABSTRACT

In the first part of given report, the properties of light and its interaction with environment are closely discussed. The light reflection and refractive index of dielectric, in our case of glass, are defined and the spectral properties of „air/film/glass“ system are described. The main emphasis is given on the utilisation of reflectometry for calculation of optical characteristics of films deposited on glass surface. The studied optical characteristics were refractive index of film and its geometric thickness. It was found that for calculation of studied characteristics of film on glass, the Eq. (1) can be used while the conditions hereinafter are valid.

At vertical incidence of light to glass with thin film, the following equation which is valid for reflectance ( $\rho$ ) of thin non-absorbing coating on glass and monochromatic radiation is defined:

$$\rho = \frac{n_1^2(n-n_0)^2 \cos^2 \frac{x}{2} + (n_1^2 - n_0n)^2 \sin^2 \frac{x}{2}}{n_1^2(n+n_0)^2 \cos^2 \frac{x}{2} + (n_1^2 + n_0n)^2 \sin^2 \frac{x}{2}} \quad (1)$$

where  $n_0$ ,  $n_1$  and  $n$  is refractive index of air, coating and glass, respectively

and  $x = \frac{4\pi}{\lambda} n_1 d \cos \varphi_1$ , where  $d$  is physical thickness of coating,  $\varphi_1$  is angle of beam incidence; in our case  $\varphi_1 \sim 0$ .

For practical usage for measurement of reflection spectra of films prepared by sol-gel method, the two approach were compared:

#### „One-side“ method

- It means that sample of glass or glass with film is edged (roughened) and covered by matt black coating on one side
- During the measurement of reflection spectrum, the reflection at back side of sample is minimized and the effect of absorption in sample is minimized too
- Obtained reflection spectrum is considered as spectrum of „air/glass“ or „air/film/glass“ system

#### „Two-side“ method

- It means that sample of glass or glass with film on both sides is measured without surface modification
- Reflection spectrum is obtained in „air/glass/air“ or „air/film/glass/film/glas/air“ system

Table 1. The comparison of „One-side“ method and „Two-side“ method

Property	One-side method	Two-side method
<i>Film</i>	AD19002Ba	jAD19002Ba
Refractive index	1.49898	1.51740
Standard deviation	$1.92538 \cdot 10^{-4}$	$2.63932 \cdot 10^{-4}$
<i>Film</i>	AD19026Va	jAD19026Va
Refractive index	1.44550	1.44681
Standard deviation	$3.47873 \cdot 10^{-3}$	$7.31993 \cdot 10^{-3}$
Thickness /nm/	97.5864	97.0998
Standard deviation /nm/	$9.60973 \cdot 10^{-1}$	1.52579
<i>Film</i>	AD19026Vb	jAD19026Vb
Refractive index	1.44837	1.44640e
Standard deviation	$1.92538 \cdot 10^{-4}$	$7.42460 \cdot 10^{-3}$
Thickness /nm/	97.5081	94.5686
Standard deviation /nm/	$7.81980 \cdot 10^{-1}$	1.58078
<i>Film</i>	TiA19001B	jTiA19001B
Refractive index	1.49840	1.50479
Standard deviation	$4.01376 \cdot 10^{-4}$	$2.61682 \cdot 10^{-4}$
<i>Film</i>	TiA19008Va	jTiA19008Va
Refractive index	2.37677	2.34183
Standard deviation	$3.67272 \cdot 10^{-2}$	$6.59529 \cdot 10^{-2}$
Thickness /nm/	108.351	106.491
Standard deviation /nm/	$6.37966 \cdot 10^{-1}$	$6.50496 \cdot 10^{-1}$
<i>Film</i>	TiA19008Vb	jTiA19008Vb
Refractive index	2.37175	2.37706
Standard deviation	$5.99867 \cdot 10^{-2}$	$6.51231 \cdot 10^{-2}$
Thickness /nm/	107.791	108.756
Standard deviation /nm/	$7.15622 \cdot 10^{-1}$	$8.17148 \cdot 10^{-1}$

On the basis of results, which are shown in Table 1, it can be concluded that observed differences between „One-side“ method and „Two-side“ method are minimal. It allows to use the „Two-side“ method for determination of refractive index and thickness of film, because the given method is significantly faster and less difficult for preparation of samples for measurement.

**Keywords:** sol-gel, inorganic-organic nanocomposite films, spectral properties, index of refraction, thickness

#### Acknowledgment:



This presentation was created in the frame of the project New materials and technologies for industry in 21st. centuries , ITMS code is 313011T546, operational program Research and innovation, co-funded from European Regional Development Fund.

## The influence of preparation conditions for inorganic-organic nanocomposite layers on their hydrophobicity

**Katarína Faturíková<sup>1</sup>, Alfonz Piško<sup>1</sup>, Jana Pagáčová<sup>2</sup>, Iveta Papučová<sup>2</sup>, Mariana Švančárková<sup>1</sup>**

<sup>1</sup> Central Laboratories, FunGlass, Alexander Dubček University of Trenčín, Študentská 2, SK-911 50 Trenčín, Slovakia

<sup>2</sup> Faculty of Industrial Technologies in Púchov, Alexander Dubček University of Trenčín, I. Krasku 491/30, SK-020 01 Púchov, Slovakia

### ABSTRACT

Glasses, which are used in architecture, can acquire new properties by functionalization. One of the possible method for functionalization is application of special layers to the glass surface and by this way the glass acquires new properties. One of the most desired properties is hydrophobicity. Wettability is determined mainly by the surface chemistry and surface topography, and it can be modified by the changing of topography such way as the application of inorganic-organic nanocomposite layers. An important method for coating of the materials is sol-gel method. This method presents many advantages such as utilization of simple equipment, high homogeneity of the thin films and the possibility of using an excessive variety of substrates and sizes. Sol-gel is a process in which the features of the layers can be controlled by varying experimental parameters such as process for mixing the reactants and temperature.

In this work, the influence of reactant addition sequence during their mixing and the reaction temperatures on hydrophobicity of layers prepared from sols in "TEOS-TriEOS-H<sub>2</sub>O-HNO<sub>3</sub>-IPA" system were observed. Simultaneously, the relationship between hydrophobicity of prepared layers and their surface properties was evaluated. The wettability properties of layers were obtained by the measurements of the contact angle of water at room temperature by sessile drop method. The morphological features and surface roughness of the thin layers were obtained by AFM measurements. Moreover, the resistance of prepared layers to water was studied, too.

**Keywords:** sol-gel, inorganic-organic nanocomposite films, contact angle, AFM, watter corrosion

### Acknowledgment:



This presentation was created in the frame of the project New materials and technologies for industry in 21st. centuries , ITMS code is 313011T546, operational program Research and innovation, co-funded from European Regional Development Fund.

## Investigation and preparation of PDC glass/ceramic coatings applied to different pre-treated stainless steel AISI441 substrates

**M. Parchovianský<sup>1</sup>, I. Parchovianská<sup>2</sup>, P. Švančárek<sup>3</sup>, D. Galusek<sup>3</sup>, G. Motz<sup>4</sup>,**

<sup>1</sup> Department of Coating Processes, FunGlass, Alexander Dubček University of Trenčín, Študentská 2, 911 50 Trenčín, Slovakia

(E-mail: milan.parchoviansky@tnuni.sk)

<sup>2</sup> Department of Functional Materials, FunGlass, Alexander Dubček University of Trenčín, Študentská 2, 911 50 Trenčín, Slovakia

<sup>3</sup> Joint Glass Centre of the IIC SAS, TnUAD and FChFT STU, FunGlass, Študentská 2, 911 50 Trenčín, Slovakia

<sup>4</sup> University of Bayreuth, Ceramic Materials Engineering, D-95440 Bayreuth, Germany

### ABSTRACT

This study describes the investigation of different cleaning procedures on AISI 441 stainless steel substrates and preparation of coatings containing passive ceramic and commercial glass fillers. In order to achieve well adherent coatings without failures, stainless steel substrates were cleaned by four different cleaning procedures. The prepared slurry was then deposited onto the steel substrate via spray coating. The experimental conditions for the pre-treatment of stainless steel are shown in Tab.1.

**Tab.1:** Experimental conditions of pre-treatment of stainless steel

Shorcut	Pre-treatment of stainless steel
U	3-steps ultrasonic vibration cleaning in acetone, ethanol and deionized water (10 min)
S	Sandblasting with glass beads (70-110 $\mu$ m), ultrasonic cleaning
K	Chemical etching – Kroll's reagent (distilled water, HNO <sub>3</sub> , HF), 20 s
S+K	Sandblasting with glass beads + etching with Kroll's reagent

The bond coat was prepared from the commercial polymer Durazane 2250 (Merck KGaA, Germany) by the dip-coating method (dip-coater RDC 15, Relamatic, Switzerland). The pyrolysis of the bond-coat was carried out in air (Nabertherm® N41/H, Nabertherm, Germany) at a temperature of 450 °C for 1 h. The top coats were prepared from the commercial polymer – Durazane 1800 (Merck KGaA, Germany), passive fillers and commercial glass. The passive fillers used were ZrO<sub>2</sub> stabilized with 8 mol. % Y<sub>2</sub>O<sub>3</sub> (8YSZ, Inframat, USA), AYZ powder and commercial glass (G018-281, Schott AG). Two compositions of top coat were prepared, C2c and D2. The prepared compositions are listed in Tab.2.

**Tab.2:** Compositions of the composite top coats after pyrolysis (vol. %)

Sample name	Durazane1800	8YSZ	AYZ	G018-281
C2c	30	35	-	35
D2	25	20	20	35

The SEM cross-sectional micrographs of compositions C2c and D2 in Fig.1 show the bonding between the bond coat and the steel substrate treated by different cleaning procedures. After pyrolysis of the coatings at 850 °C irrespective of the cleaning process applied, the bond coat did not delaminate from the steel surface, indicating its good adhesion to the metal substrate. An intact bond coat approximately 1  $\mu$ m thick was observed in all cases. The top coat layers of both studied compositions, C2c and D2, were almost dense, with only small closed pores observed.

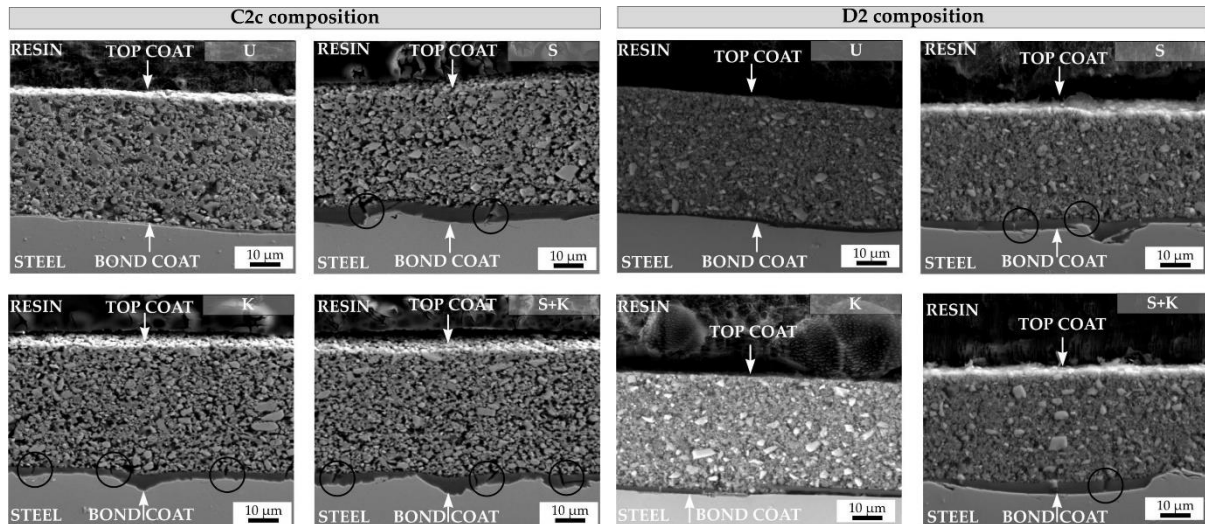


**Fig. 1:** SEM cross-section of pyrolysed C2c and D2 coatings. The applied cleaning procedure is indicated by the abbreviation in the upper right corner of each figure.

SEM cross-sections of C2c and D2 compositions after corrosion tests are shown in Fig.2. In all cases, except for ultrasonic cleaning, during the corrosion tests the bond coat delaminated from the surface of stainless steel. Chemical etching of the steel surface with the Kroll's solution probably caused changes in the microstructure and chemical composition of the steel, resulting in peeling of the coating. For samples with a sandblasted surface treatment, or a combination of sandblasting and etching, the bond coat and the top coat were detached because of the high surface roughness, although it was assumed that such a surface treatment would lead to the highest adhesion. Simple cleaning by ultrasonication in acetone, ethanol and deionised water is the most effective way for achieving a sufficient bonding of the bond coat to the steel substrate after corrosion tests.

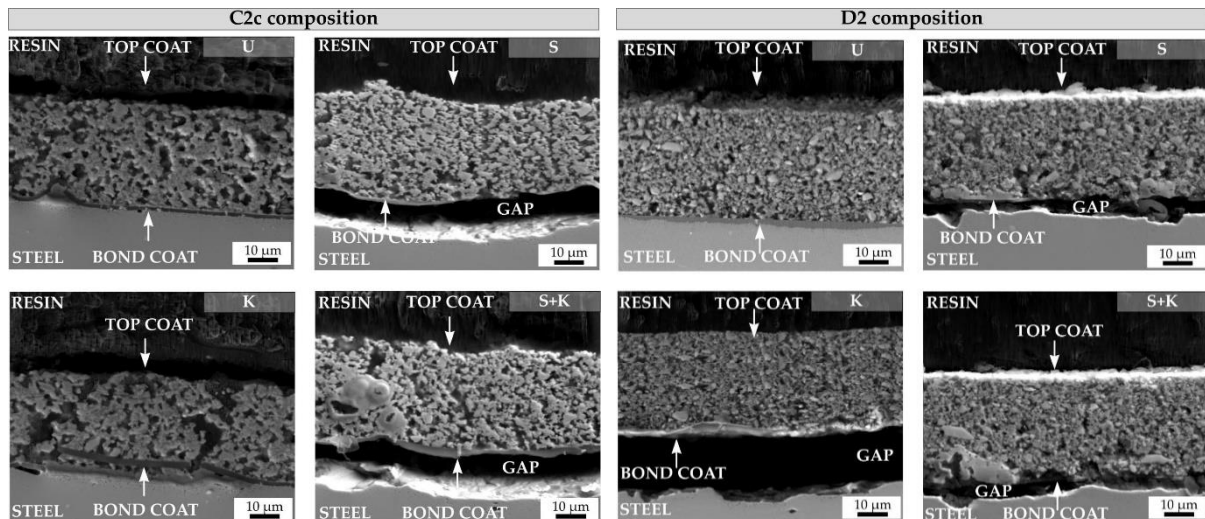


**Fig. 2:** SEM cross-section of C2c and D2 compositions after corrosion tests. The applied cleaning procedure is indicated by the abbreviation in the upper right corner of each figure

**Keywords:** Polymer derived ceramics, bond coat, passive fillers, corrosion

#### Acknowledgment:



Financial support of this work by the APVV 0014-15 grant and the Deutscher Akademischer Austauschdienst (DAAD) grant scheme is gratefully acknowledged. This paper was also created in the frame of the project Centre for Functional and Surface Functionalized Glass (CEGLASS), ITMS code is 313011R453, operational program Research and innovation, co-funded from European Regional Development Fund.

## Sol-gel based hybrid coatings for corrosion protection of AA2024-T3 alloys

**N. Afsharimani<sup>1</sup>, Y. Castro<sup>2</sup>, A. Duran<sup>2</sup> and D. Galusek<sup>1</sup>**

<sup>1</sup> Department of Coating Processes, FunGlass, Alexander Dubček University of Trenčín, Študentská 2, 911 50 Trenčín, Slovakia

(E-mail:nasima.afsharimani@tnuni.sk)

<sup>2</sup> Departamento de Vidrios, Instituto de Cerámica y Vidrio (ICV), Consejo Superior de Investigaciones Científicas(CSIC), C/ Kelsen nº 5, Campus de Cantoblanco (UAM), 28049 Madrid, Spain

### ABSTRACT

Hybrid sol-gel coatings were synthesized and studied in the present work as pre-treatments for the aluminum alloy AA2024-T3 to provide corrosion protection in 0.05 M NaCl solution. The pristine sol-gel films were prepared from Tetraethoxysilane (TEOS) and 3-glycidoxypropyl-trimethoxysilane (GPTMS) precursors. The coatings synthesis protocol was further developed by incorporation of graphene nanosheets and colloidal SiO<sub>2</sub> nanoparticles with the aim of improving the structural properties such as coating integrity and barrier properties against corrosive medium. To this end, graphene nanosheets were modified through a straightforward hydrothermal approach which resulted in compatible and stable dispersion of nanosheets into GPTMS/TEOS sols (Fig.1). Additionally, the hybrid sols were doped with colloidal SiO<sub>2</sub> (Ludox) nanoparticles to achieve dense and defect free structures. Optimization of sol synthesis was based on the results of ATR-FTIR and UV-vis-NIR spectroscopies. Opening of epoxy rings and completion of hydrolysis and condensation reactions during the synthesis process were also confirmed. Coatings were characterized through thickness, water contact angle, and electrochemical properties (potentiodynamic polarization).

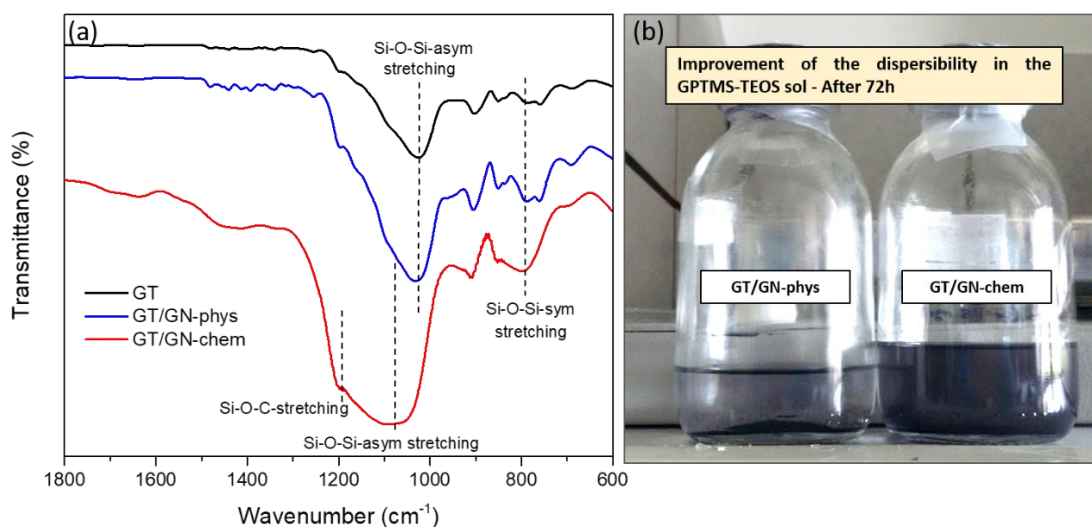


Fig. 1. (a) FTIR spectra of pristine GPTMS/TEOS (GT, black curve), GPTMS/TEOS doped with graphene nanosheets before chemical modification (GT/GN-phys, blue curve) and GPTMS/TEOS doped with chemically modified graphene nanosheets (GT/GN-chem, red curve) and (b) visual image of dispersion improvement of graphene nanosheets in GPTMS/TEOS sols after chemical modification.

The results showed that the incorporation of graphene nanosheets into hybrid sol-gel coatings affected the corrosion properties. According to surface chemical, structural and electrochemical characterizations, incorporation of chemically modified graphene nanosheets into TEOS and GPTMS sols including colloidal SiO<sub>2</sub> led to the better corrosion protection properties compared to those with graphene nanosheets embedded in pure TEOS and GPTMS sols. The coatings based on chemically modified graphene and SiO<sub>2</sub> nanoparticles appeared to be thicker (thickness =  $5.5 \pm 0.2$   $\mu\text{m}$ ) and rougher (average roughness =  $7.4 \pm 0.1$  nm) with reduced hydrophilicity (water contact

angle =  $74 \pm 2^\circ$ ). According to polarization measurements, promising passive (barrier) ranges were formed for such coatings and corrosion current densities decreased down to values almost  $\sim 10^5$  times smaller than that of the bare AA2024-T3 alloy (Fig.2). Such encouraging barrier properties could originate from the both layered graphene structure and the presence of  $\text{SiO}_2$  nanoparticles that likely reduced the active surface area of the coating accessible for the attack of the corrosive medium through perhaps reinforcing the cross-linking density. These coatings could be promising candidates to be applied on the surface of AA2024-T3 alloys combined with deposition of an organic top coat for corrosion protection applications.

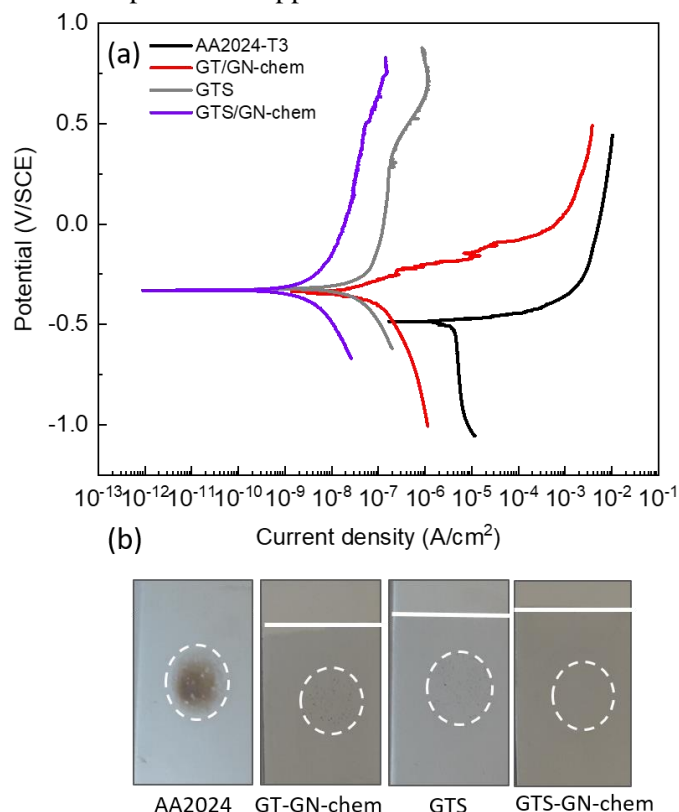


Fig. 2 (a) Potentiodynamic polarization curves of bare AA2024-T3 alloy (black curve) and samples coated with hybrid sol-gel coatings including GPTMS/TEOS doped with chemically modified graphene nanosheets (GT/GN-chem, red curve), GPTMS/TEOS/colloidal  $\text{SiO}_2$  (GTS, grey curve) and GPTMS/TEOS/colloidal  $\text{SiO}_2$  doped with chemically modified graphene nanosheets (GTS/GN-chem, purple curve) and (b) visual images of corroded surface areas (white dashed circles) after exposure to corrosive medium (0.05 M NaCl). For a better visibility, the white lines indicate the boarder between the coated and uncoated areas. As it is visible to the naked eye, the sample with GTS-GN-chem coating shows the least surface damage compared to the bare alloy.

**Keywords:** Aluminum alloy, Sol-gel coatings, Corrosion protection, Barrier properties,  $\text{SiO}_2$  nanoparticles, Graphene nanosheets

#### Acknowledgement:



This paper is a part of dissemination activities of project [FunGlass](#). This project has received funding from the European Union's Horizon 2020 research and innovation programme under grant agreement No 739566.

## High temperature oxidation behavior of AISI441 stainless steel and PDC coatings in synthetic air atmosphere

**I. Parchovianská<sup>1</sup>, M. Parchovianský<sup>1</sup>, P. Švančárek<sup>1</sup>, G. Motz<sup>2</sup> and D. Galusek<sup>1, 3</sup>**

<sup>1</sup> FunGlass - Centre for Functional and Surface Functionalized Glass, Študentská 2, 911 50 Trenčín, Slovakia

(E-mail: ivana.parchovianska@tnuni.sk)

<sup>2</sup> University of Bayreuth, Ceramic Materials Engineering (CME), D-95440 Bayreuth, Germany

<sup>3</sup> Joint Glass Centre of the IIC SAS, TnUAD and FChFT STU, Bratislava, Slovakia

### ABSTRACT

This work features the oxidation behaviour of ferritic stainless steel grade AISI 441 coated with protective polymer derived ceramic coatings (PDC). Two PDC layers were studied with respect to their oxidation resistance in the atmosphere of synthetic air at temperatures of up to 1000 °C. The coatings contain three passive fillers: yttria-stabilized zirconia (8-YSZ, Inframat, USA), alumina-yttria-zirconia (AYZ) powder prepared via Pechini sol-gel route, and the commercial seal glass (G018-281, Schott AG). The process began with a pre-treatment of the steel substrates using ultrasonication in acetone and the preparation of the coating slurry. Subsequently, the perhydropolysilazane-based bond coat was applied via dip-coating and fixed by pyrolysis at 450 °C before the composite top coat was spray-coated and again pyrolysed in air at 850 °C. The top coats were prepared from the commercial polymer - Durazane1800 (Merck KGaA, Germany), passive fillers and commercial glass. The details of the coatings selected for oxidation testing are summarized in Tab. 1. Next, oxidation tests were performed in a horizontal electric tube furnace at 900, 950 and 1000 °C with exposure times of 24 h and 96 h in flowing synthetic air. The oxidation behaviour was evaluated by weight change measurements, which compare the mass change of coated and uncoated substrates (Tab. 2). The degree of corrosion was also investigated by scanning electron microscopy (SEM) using a JEOL JSM 7600 F (JEOL, Japan).

Tab. 1: Compositions of the produced coatings before pyrolysis (vol. %) and their estimated thermal expansion coefficients (CTE, 10<sup>-6</sup>/K)

Composition	Durazane1800	YSZ	AYZ	G018-281	CTE
C2	30	35	-	35	10.1
D4	30	1.5	17.5	35	9.4

A significant weight gain of the unprotected steel was measured after all experiments due to the oxide scale growth on its surface. The small weight loss observed from the C2-coated steel after 24 h and 96 h at 900 °C can be attributed to an error in weight measurement (the total weight change is <10 mg). This also applies for the negligible weight losses measured for the D4 coated steels exposed for 24 h at 900 °C and 950 °C. After exposures to oxidative atmosphere at 950 °C and 1000 °C, the C2-coated steels showed a dramatic increase of the weight loss, indicating the total coating failure, while oxidation tests of the D4-coated steel showed a small weight gain after exposure at 950 °C and 1000 °C.

Tab. 2: Weight changes of stainless steel substrates and PDC coatings at different temperatures and times after oxidation tests (mg/cm<sup>2</sup>)

		900 °C	950 °C	1000 °C
Uncoated steel	24 h	0.21	0.44	0.72
	96 h	0.45	0.77	1.21
C2 coating	24 h	-0.11	-1.33	-4.95
	96 h	-0.14	-5.07	-5.48
D4 coating	24 h	-0.05	-0.03	0.03
	96 h	0	0.15	0.27

SEM micrograph illustrating the surface of the uncoated steel after oxidation tests at 950 °C and exposure time of 24 h is shown in Fig. 1a). The whole surface is covered with small particles of oxidation products, which were detected by XRD and EDS to be  $(\text{Mn, Cr})_3\text{O}_4$  spinel,  $\text{Cr}_2\text{O}_3$  and  $\text{TiO}_2$ . Cross-sections of the protective coatings C2 and D4 after exposure to 950 °C for 24 h are presented by the SEM-micrographs in Fig. 1b), c). In the case of C2 coating, exposure time of 24 h to 950 °C led to progressive cracking along the metal/coating interface (marked with white arrows in Fig. 1b). Long exposure to 950 °C and 1000 °C led to an entire coating delamination, as indicated by abrupt increase in the weight loss.

The optimised composite coating D4 yielded the most promising results after oxidation tests. The D4 coating exhibited lower porosity than C2 coating. Moreover, no continuous cracks across the coating were detected. No significant corrosion damage was observed in D4 coating after oxidation tests: the coating acts as the robust oxidation protection system. This indicates that specially tailored AYZ passive filler with an adjusted CTE ensured its compatibility with the composite ceramic coating with respect to its thermal properties. Suppression of crack formation during oxidation testing was thus achieved.

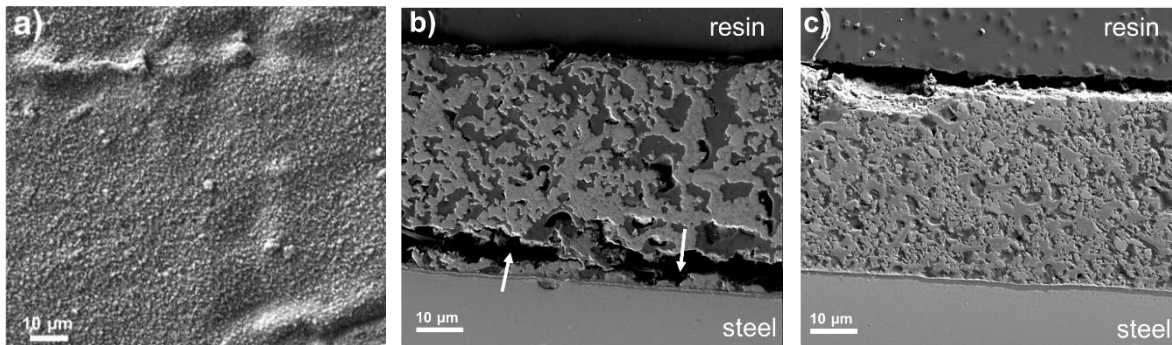


Fig. 1: SEM micrographs of samples exposed to oxidation at 950 °C for 24h: a) uncoated steel surface, b) C2 cross section, c) D4 cross section

**Keywords:** high-temperature oxidation, PDC coatings, stainless steel

#### Acknowledgment:



Financial support of this work by the APVV 0014-15 grant and the Deutscher Akademischer Austauschdienst (DAAD) grant scheme is gratefully acknowledged. This paper was also created in the frame of the project Centre for Functional and Surface Functionalized Glass (CEGLASS), ITMS code is 313011R453, operational program Research and innovation, co-funded from European Regional Development Fund.

## Corrosion resistance hybrid sol gel coating: its synthesis and characterizations

Nitin Kamble<sup>1</sup>, Yolanda Castro<sup>2</sup> Alicia Durán<sup>2</sup> and Dušan Galusek<sup>1</sup>

<sup>1</sup> FunGlass, Alexander Dubček University of Trenčín  
(E-mail: nitin.kamble@tnuni.sk)

<sup>2</sup> Instituto de Cerámica y Vidrio, CSIC

### ABSTRACT

Hybrid organic/inorganic structures show excellent mechanical, thermal and optical properties, combining the stability of ceramic materials with the flexibility of polymeric ones. During the last few years, effort has been devoted to the synthesis of hybrid polymers obtained by reaction with organic and inorganic compounds due to the remarkable properties of these materials [1-3]. Protective organic coatings are widely employed as primers to protect steel surfaces from corrosion. However, poor adhesion of the coating material to the steel can cause not only delamination of the coating material, but the corrosion of the steel substrate beneath the coating material. On the other hand, protective inorganic coatings can provide excellent properties in thermal shock resistance, creep resistance, high temperature strength and thermal stability. Metal oxidation is one of the main problems found in industry and interest in the production of protective coatings has increased. Several materials have been applied to solve this problem, including organic and inorganic polymers.

Hybrid polymers are a very interesting and promising area of study. Alkoxy group-functionalized amorphous silica-based inorganic-organic hybrid materials were designed and synthesized from PHPS by chemical modification. The sol-gel matrix was produced from, tetraethoxysilane (TEOS), hybrid precursor organically functionalized PHPS. The evolution of the solutions, mainly the chemical structure, during the processes of hydrolytic condensation and organic polymerization was studied as a function of the sol concentration through Fourier transformed infrared spectroscopy (FTIR). Single layer will be deposited on glass substrate by chemical dip coating method.

Polysilazane bands at  $\sim 3385\text{ cm}^{-1}$  (N–H stretching mode),  $\sim 2950\text{ cm}^{-1}$  (C–H symmetric stretching mode),  $\sim 2125\text{ cm}^{-1}$  (Si–H symmetric stretching mode),  $\sim 1250\text{ cm}^{-1}$  (C–H symmetric deformation mode) and  $\sim 1150\text{ cm}^{-1}$  (N–H bending mode) [4,5]. After the selective crosslinking reactions, the bands concerning N–H and Si–H groups became smaller, indicating the consumption of these functional groups. The decrease of a broad peak at  $\sim 3400\text{ cm}^{-1}$  corresponding to OH groups also confirms that formation of Si–O–Si bond [6] which is indicated in fig.1 a) and 1b). In Fig.2 a) and b) shows area under curve and area decreases as reaction time increases. Firstly, the Si–H groups react rapidly with water, forming Si–OH groups and generating hydrogen molecules. In the next step, the silanol intermediates may react with each other by condensation to siloxane units and the formed water molecules attack the Si–N bonds, which again generates silanol groups. This reaction creates a dense hybrid silica network.

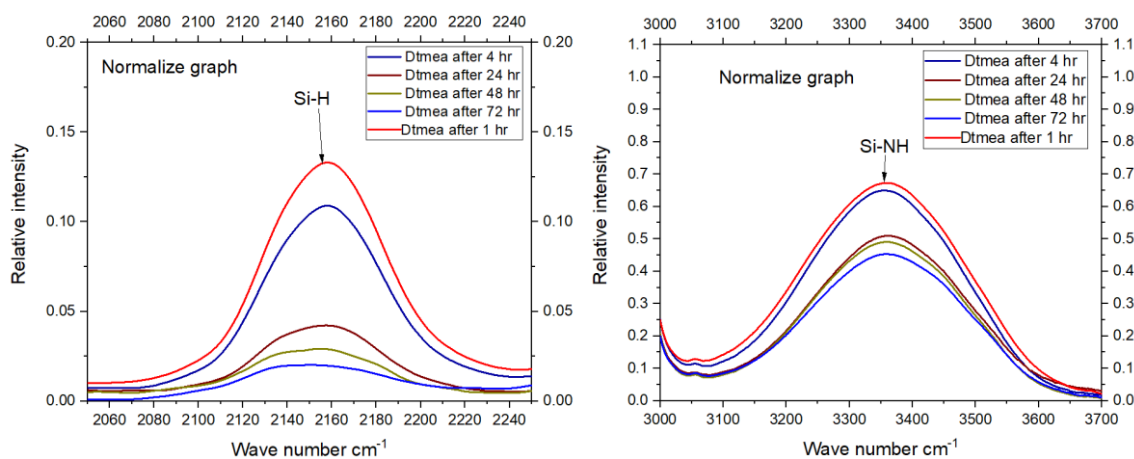


Fig.1: a) FTIR spectra of Si-H peak b) FTIR spectra of Si-NH peak.

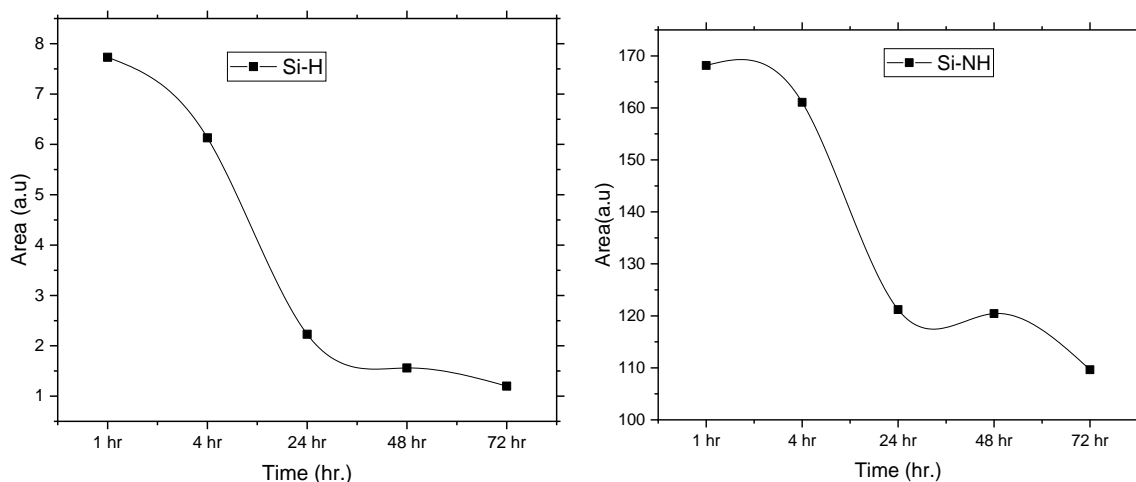


Fig.2: a) Area under curve of Si-H peak b) Area under curve of Si-NH peak

**Conclusion:** Crack-free and optically transparent hybrid organic–inorganic coatings were deposited onto glass from sol prepared by acid-catalyzed hydrolytic polycondensation of TEOS, MPS and Durazane mixtures, at various TEOS/MPS/Durazane molar ratios, followed by radical polymerization of Aibn. FTIR results showed that the degree of polycondensation increases as the synthesis time increases and the formation of very strong Si–O–Si bonds, while the extent of organic polymerization is essentially unaffected by the amount of acid and ethanol concentration. Maximum coating thickness till now obtained upto 1  $\mu\text{m}$  through this hybrid sol.

#### Acknowledgment:



This item is a part of dissemination activities of project [FunGlass](#).  
This project has received funding from the European Union's Horizon 2020 research and innovation programme under grant agreement No 739566.

- References:** [1] E. Rubio, J. Almaral, R. Ramírez-Bon, V. Castaño, V. Rodríguez, *Opt. Mater. (Amst.)*, 27 (2005), 1266-1269,  
[2] N.M. José, L.A.S.A. Prado, *Quim. Nov.*, 28 (2005), 281-288,  
[3] K.E. Lee, N. Morad, T.T. Teng, B.T. Poh, *Chem. Eng. J.*, 203 (2012), 370-386  
[4] R. Chavez, I. Ionescu, C. Balan, C. Fasel, R. Riedel, *J. Appl. Polym. Sci.*, 119 (2011), 794-802  
[5] O. Flores, T. Schmalz, W. Krenkel, L. Heymann, G. Motz, *J. Mater. Chem. A*, 1 (2013), 15406-15415.  
[6] M. Günthner, K. Wang, R. K. Bordia and G. Motz, *J. Eur. Ceram. Soc.*, 32, (2012), 1883–1892

## Porous Bioactive Glass Microspheres Prepared by Flame Synthesis

**J. Kraxner<sup>1</sup>, M. Michalek<sup>1</sup>, A. R. Romero<sup>2</sup>, H. Elsayed<sup>2</sup>,  
E. Bernardo<sup>2</sup> and D. Galusek<sup>3</sup>**

<sup>1</sup> FunGlass, Alexander Dubček University of Trenčín, Trenčín, Slovakia  
(E-mail: jozef.kraxner@tnuni.sk)

<sup>2</sup> Department of Industrial Engineering, Università degli Studi di Padova, Padova, Italy

<sup>3</sup> Joint glass centre of the IIC SAS, TnUAD, and FChFT STU, FunGlass, Alexander Dubček University of  
Trenčín, Trenčín, Slovakia

### ABSTRACT

Low cost processing method to prepare porous bioactive glass (BG) microspheres is presented. Glass powder with composition based on 45S5 BG and exhibiting irregularly shaped particles was fabricated by conventional melting. Glass powder was alkali activated to induce pore formation during the following flame synthesis step. Porous microspheres, with diameters ranging between 45 and 75  $\mu\text{m}$ , were successfully prepared and characterized by X-ray diffraction, Fourier-transform infrared spectroscopy, and scanning electron microscopy with energy-dispersive X-ray spectroscopy. The porous bioactive glass microspheres are promising candidates for applications in bone regeneration, tissue engineering, and as carriers for controlled drug delivery.

The field of inorganic bioactive materials started in 1971 with the discovery of 45S5 bioactive glass (BG) by Hench et al. [1]. It is a special composition of silicate glass containing 45%  $\text{SiO}_2$ , 24.5%  $\text{CaO}$ , 24.5%  $\text{Na}_2\text{O}$ , and 6%  $\text{P}_2\text{O}_5$ , in wt.%. Bioactive glass is able to bond to bone tissue and stimulates bone regeneration by the release of Si, Ca, P ions [2, 3]. Due to the low specific surface area, and the lack of microporosity, the bioactivity of melt-derived glasses mainly depends on the  $\text{SiO}_2$  content [4]. Microspheres possess several advantages compared to irregularly shaped materials; therefore, they have become important in many scientific fields, including biomaterials. They can be engineered and manufactured to be solid, hollow, or porous, which provides a larger surface area allowing for sufficient therapeutic coatings, an increase in degradation rate and beneficial ion release profile [5], or encapsulation of various biomedical relevant components [6, 7]. Recently, porous calcium phosphate glass microspheres were fabricated by Hossain et al. [6] via the cost-effective flame spheroidisation process. Careful selection of the glass, pore-forming agent, and a manufacturing method with the required processing window enabled the production of porous glass microspheres via a single-stage manufacturing process. Microspheres are already exploited in the pharmaceutical and health care industry. Precise control over pore size is, however, difficult; hence, manufacturing technologies need to be improved to create reproducible porosity and pore sizes [7]. In the present study, a simple, cost-effective, and scalable method for the preparation of porous 45S5 BG microspheres is presented and discussed.

Bioactive glass of 45S5 composition was prepared by mixing the analytical grade purity ( $\geq 99\%$ ) raw materials:  $\text{SiO}_2$ ,  $\text{CaCO}_3$  (Centralchem, Slovakia),  $\text{Na}_2\text{CO}_3$  (Penta, Czech Republic), and  $\text{Na}_5\text{P}_3\text{O}_{10}$  (Sigma-Aldrich, Slovakia). The mixture was then melted in Pt-10% Rh crucible in a superkanthal furnace at  $1300^\circ\text{C}$  for two hours in ambient atmosphere. The homogeneity was ensured by repeated hand mixing of the melt. Then the molten glass was poured onto a stainless steel plate. The sample was tempered in a muffle furnace for 30 minutes at  $560^\circ\text{C}$  and then the furnace was switched off. The prepared bulk glass was crushed and sieved through a  $45\ \mu\text{m}$  analytical sieve. The powder was mixed into an aqueous solution containing 1 M NaOH (reagent grade, Sigma Aldrich, UK), with a solid loading of 65 wt%. The glass powder was subjected to an alkaline attack for 1 h under mechanical stirring at 500 rpm. After alkaline activation, the obtained suspension of glass powders, subjected to surface dissolution, was cast in closed polystyrene cylindrical moulds and cured at  $75^\circ\text{C}$  for 24 hours. Finally, the hardened gel was crushed and sieved through analytical sieves to obtain fraction of 45-75  $\mu\text{m}$  in size.

The precursor, prepared by the alkaline activation process, was fed into an oxygen-methane torch with a vacuum powder feeder using oxygen carrier gas. The spherical melt particles were formed in the flame with the estimated maximum temperature in the range of 1500-1600°C (which was measured in the centre of flame by a thermocouple) and then quenched by distilled water to form porous microspheres. The obtained spherical particles were separated from the distilled water by microfiltration through a ceramic filter with the pore size less than 0.3 µm.

To the best of our knowledge the paper presents the first successful preparation of porous bioactive (Figure 1) glass microspheres based on 45S5 BG composition by flame synthesis process. The microspheres were prepared by alkaline activation of conventionally melted BG powder, followed by flame spheroidisation. C-S-H and natrite, formed during the alkaline activation release volatile species (water vapour and CO<sub>2</sub>) during the flame synthesis, which act as pore forming agents yielding to porous microspheres with diameter ranging between 45 and 75 µm. Only slight reduction in the content of Na<sub>2</sub>O, P<sub>2</sub>O<sub>5</sub>, and CaO was observed after the flame synthesis.

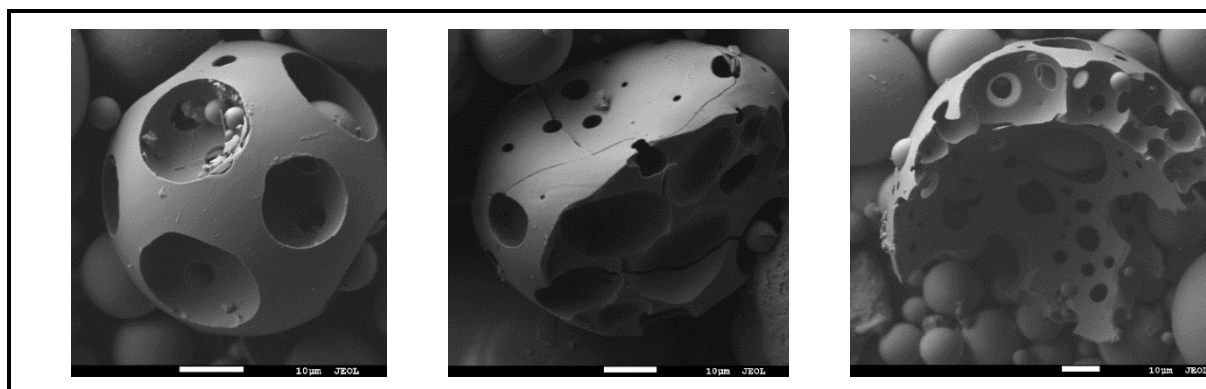


Figure 1: Morphology of the as prepared porous 45S5 BG micro-sphere particles.

**Keywords:** Bioactive glass, porous microspheres, alkaline activation, flame synthesis.

#### Acknowledgment:



This item is a part of dissemination activities of project [FunGlass](#). This project has received funding from the European Union's Horizon 2020 research and innovation programme under grant agreement No 739566.

#### References:

- [1] L. L. Hench, et al.: Bonding Mechanisms at the Interface of Ceramic Prosthetic Materials, *Journal of Biomedical Materials Research* 5 (1971) 117-141.
- [2] J. R. Jones: Reprint of: Review of bioactive glass: From Hench to hybrids, *Acta Biomaterialia* 23 (2015) S53 S82.
- [3] A. Hoppe, N. S. Guldal, A. R. Boccaccini: A review of the biological response to ionic dissolution products from bioactive glasses and glass-ceramics, *Biomaterials* 32 (2011) 2757-2774.
- [4] C. T. Wu and J. Chang, Multifunctional mesoporous bioactive glasses for effective delivery of therapeutic ions and drug/growth factors, *Journal of Controlled Release* 193 (2014) 282-295.
- [5] S. Li et al.: Porous-wall hollow glass microspheres as novel potential nanocarriers for biomedical applications, *Nanomedicine: Nanotechnology, Biology and Medicine* 6 (2010) 127-136.
- [6] K. M. Z. Hossain et al.: Porous calcium phosphate glass microspheres for orthobiologic applications, *Acta Biomaterialia* 72 (2018) 396-406.
- [7] K. M. Z. Hossain, U. Patel, I. Ahmed: Development of microspheres for biomedical applications: a review, *Progress in Biomaterials* 4 (2015) 1-19.

## Method for producing 3D silicate based bioactive glass-ceramic scaffolds using digital light processing

**Arish Dasan<sup>a</sup>, Hamada Elsayed<sup>b,c</sup>, Jozef Kraxner<sup>a</sup>, Dusan Galusek<sup>d</sup>, Paolo Colombo<sup>c</sup>, Enrico Bernardo<sup>c</sup>**

<sup>a</sup>Department of Glass Processing, FunGlass, Alexander Dubček University of Trenčín, Študentská 2, 911 50 Trenčín, Slovakia  
(E-mail: arish.dasan@tuni.sk)

<sup>b</sup>Ceramics Department, National Research Centre, Cairo, Egypt

<sup>c</sup>Department of Industrial Engineering, Università degli Studi di Padova, Padova, Italy

<sup>d</sup>Joint glass centre of the IIC SAS, TnUAD, and FChFT STU, FunGlass, Alexander Dubček University of Trenčín, Trenčín, Slovakia

### ABSTRACT

In the field of bone tissue engineering, silicate based bioactive ceramics have been extensively studied due to their bone-like apatite-formation ability when implanted into bone [1]. Recently, there is an increasing interest in highly porous scaffolds, seeking for effective osteoconduction, which mainly depends on the total porosity of the scaffolds, pore size and interconnected pore distribution that allows cellular migration, diffusion of nutrients and metabolites and the proper angiogenesis [2].

Advancements in additive manufacturing (AM) of bioactive materials enable complex porous geometries and net or near-net shape products to be fabricated to high accuracy without tooling such as moulds. Digital light processing is a lithography based technology that requires a photo-curable organic or inorganic resin (it has the special property of being able to become solid once it is exposed to light) as a matrix. Photo-curable silicone resin not only gives the final product shape, but also it yields ceramic/glass component known also as polymer derived ceramics (PDCs). By heat treatment it converts to SiOC or/and SiC in inert and to SiO<sub>2</sub> in ambient atmosphere [3]. Although some photo-curable silicones are already commercially available, the low ceramic yield (causing cracks and uncontrolled volume shrinkage), high costs and processability (require heavy metal traces containing photo catalytic initiator which, that would affect the biological activity) are critical parameters and need to be improved.

It has been reported that mixing of silicone resins with reactive oxide fillers after suitable thermal treatment yields silicate based bioceramics. Åkermanite (Ca<sub>2</sub>MgSi<sub>2</sub>O<sub>7</sub>) 3D scaffolds with hierarchical porosity, i.e. macroporosity resulting from the applied AM technology and nanoscale pores resulting from the processing route) were prepared by direct ink writing of silicone resin mixed with CaCO<sub>3</sub> and MgO/Mg(OH)<sub>2</sub>, after heat treatment at 1100°C. The achievement of phase purity is enhanced by the introduction of borate salts, providing liquid phase upon firing and promoting ionic interdiffusion [4].

The present study describes the method to produce 3D printed SiOC and Åkermanite porous scaffolds with complex shapes by digital light processing of a photocurable slurry consisting of engineered silicone mixtures. Considering the difficulties of using photocurable silicones, simple blending of commercial photo insensitive silicones with a sacrificial photocurable organic resin was applied as an alternative. Three commercial silicone resins (namely MK, H44 and H62C from Wacker Chemie AG) were selected and tested in order to ensure stable photocurable blends. The blends were further refined with the introduction of fillers (CaCO<sub>3</sub> and MgO/Mg(OH)<sub>2</sub>), followed by firing at 1100 °C, in air to obtain complex shaped Åkermanite scaffolds. Optimized samples (from H44 resin) and reactive fillers (including up to 4.5wt% borax additive), led to crack-free, phase-pure scaffolds, with microporous struts.

**Keywords:** biomaterials; silicones; digital light processing; additive manufacturing; Åkermanite.

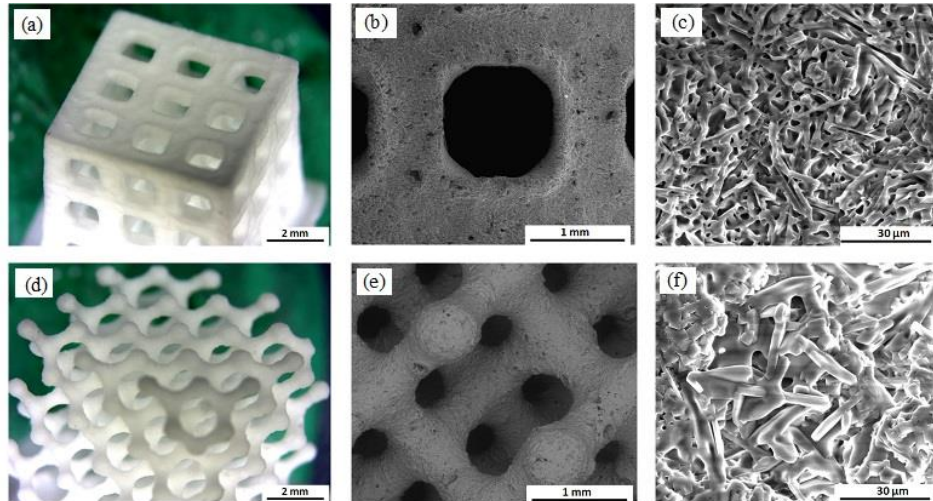


Fig.1 Optical and SEM images (cubic (a,b,c) and diamond (d,e,f) models) of H44 derived Åkermanite scaffolds

#### References:

- [1] Huang Y, Wu C, Zhang X, Chang J, and Dai K, Regulation of immune response by bioactive ions released from silicate bioceramics for bone regeneration, *Acta Biomater.*, 66, 2018, 81–92.
- [2] Tia JK, Natalie CH, Stephanie E, Jutta YM, Daniella MF, Ukrit T, Himanshu J and Matthias MF, New bioactive glass scaffolds with exceptional qualities for bone tissue regeneration: response of osteoblasts and osteoclasts, *Biomed. Mater.*, 2018, 13, 025005.
- [3] Johanna S, Paolo C, Digital light processing of ceramic components from polysiloxanes, *J. Eur. Ceram. Soc.*, 2018, 38, 57-66
- [4] Arish D, Hamada E, Jozef K, Dusan G, Enrico B, Hierarchically porous 3D-printed akermanite scaffolds from silicones and engineered fillers, *J. Eur. Ceram. Soc.*, 2019, 39, 4445-4449

#### Acknowledgment:



This publication was created in the frame of the project Centre for Functional and Surface Functionalized Glass (CEGLASS), ITMS code is 313011R453, operational program Research and innovation, co-funded from European Regional Development Fund.

## Influence of aluminosilicates and their modified forms on properties of composite materials

**B. Pecušová<sup>1</sup>, M. Pajtášová<sup>2</sup>, A. Prnová<sup>3,4</sup>, J. Valúchová<sup>3,4</sup>**

<sup>1</sup> Central Laboratories, FunGlass, Alexander Dubček University of Trenčín, Študentská 2, SK-911 50 Trenčín, Slovakia  
(E-mail: beata.pecusova@tnuni.sk)

<sup>2</sup> Faculty of Industrial Technologies in Púchov, Alexander Dubček University of Trenčín,

<sup>3</sup> VILLA – Joined Glass Centre of the IIC SAS, TnUAD, FchPT STU, Študentská 2, SK-911 50 Trenčín, Slovakia

<sup>4</sup> VILLA, FunGlass, Alexander Dubček University of Trenčín, Študentská 2, SK-911 50 Trenčín, Slovakia

### ABSTRACT

Influence of aluminosilicates and their modified forms on properties of composite materials (especially rubber blends) was studied in this work. Modified  $\text{Co}^{2+}$ ,  $\text{Cu}^{2+}$  and  $\text{Ni}^{2+}$  forms were prepared from commercial bentonite, kaolin and illite based clay products. On the second step, organomodified forms were prepared by intercalating the organic molecules of dithiophosphate and benzthiazole sulfur vulcanization accelerators. Clay products and their modified and organomodified forms were studied and characterized by thermal gravimetric (TG/DTG) analysis (Fig.1), infrared (IR)spectroscopy (Fig.2) and X-ray powder diffraction (XRD) analysis (Fig.3).

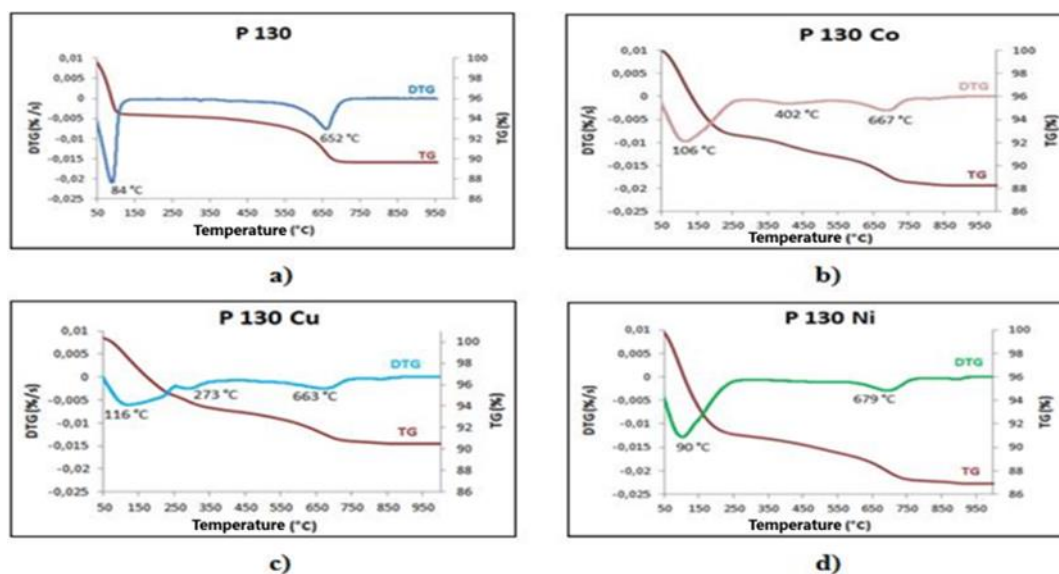


**Fig. 1** TG and DTG curves of bentonite sample P 130 and its modified forms a) P 130, b) P 130 Co, c) P 130 Cu, d) P 130 Ni

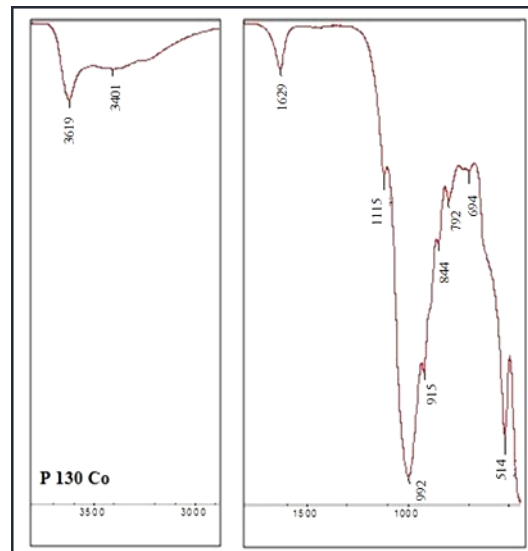


**Fig. 2** IR spectrum of modified sample P 130 Co

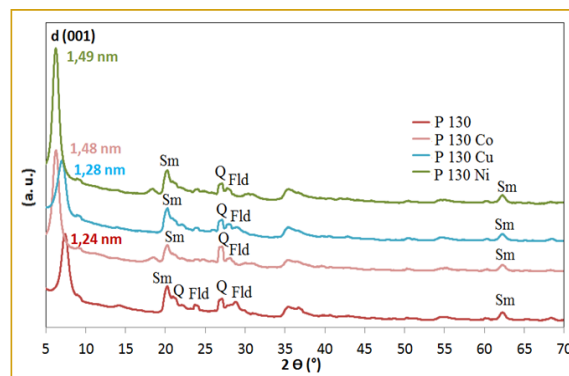


**Fig. 3** X-ray diffraction patterns of sample P130 and modified forms P130 Co, P130 Cu and P130 Ni

Finally, by both ways modified clay materials were applied to the tread rubber blends as fillers. The influence of these materials on the vulcanization characteristics of the blends was studied and impact on the physical-mechanical properties before and after aging and the resilience flexibility for the preparing vulcanizates were evaluated. The possibility of modified and organomodified clay products application in composite materials has been successfully demonstrated.

The obtained results of this work provide new knowledge on the use of modified and organomodified clay products as fillers.

**Keywords:** aluminosilicates, composite materials, fillers, spectral and thermal properties, vulcanization characteristics, physical-mechanical properties.

#### Acknowledgment:



This presentation was also created in the frame of the project Centre for Functional and Surface Functionalized Glass (CEGLASS), ITMS code is 313011R453, operational program Research and innovation, co-funded from European Regional Development Fund.

## Mesoporous bioactive glass doped with therapeutic inorganic ions

**Martin Michálek<sup>1</sup>, Fatih Kurtuldu<sup>1</sup>, Zuzana Neščáková<sup>1</sup>, Liliana Liverani<sup>2</sup>, Dušan Galusek<sup>3</sup> and Aldo R. Boccaccini<sup>2</sup>**

<sup>1</sup> Department of Biomaterials, FunGlass, Alexander Dubček University of Trenčín, Študentská 2, 911 50 Trenčín, Slovakia

<sup>2</sup> Department of Materials Science and Engineering, University of Erlangen – Nuremberg, 910 58 Erlangen, Germany

<sup>3</sup> Dpt. VILA – Joint Glass Centre of the IIC SAS, TnUAD, FChPT STU, Študentská 2, 911 50 Trenčín, Slovakia, FunGlass, A. Dubček University of Trenčín, Študentská 2, 911 50 Trenčín, Slovakia

### ABSTRACT

In the present study the mesoporous bioactive glass (MBG) particles were prepared by micro-emulsion assisted sol-gel technique. Incorporation of therapeutic inorganic ions (TII) enhance the biological impact of MBG materials. Metallic ions such as strontium, copper, gallium, cerium, magnesium and boron have been incorporated to the binary system SiO<sub>2</sub> / CaO with the nominal composition of 60/40 mol %. The effect of TII doping on the morphology and chemical composition of MBG nanoparticles was investigated. Using the microemulsion assisted sol-gel preparation technique the influence of Sr<sup>2+</sup>, B<sup>3+</sup>, Mg<sup>2+</sup>, Cu<sup>2+</sup>, Ga<sup>3+</sup> and Ce<sup>3+</sup> dopants on the morphology and chemical composition has been studied. The used dopants have a significant effect on the size, shape and chemical composition when the conditions of the sol-gel process are fixed. The presented results will help to understand better the effect of therapeutic inorganic ions incorporation into the bioactive glasses, in aim to fully reveal their potential in the field of biomedical applications such as bone, soft tissue engineering, drug loading, etc.

**Keywords:** sol-gel, mesoporous bioactive glass, therapeutic ions, morphology, bioactivity

### ACKNOWLEDGMENT



This paper is a part of dissemination activities of the project FunGlass. This project has received funding from the European Union's Horizon 2020 research and innovation programme under grant agreement No 739566. Financial support of this work by the grants SAS-MOST JRP 2018/02 and VEGA 1/0098/19 is gratefully acknowledged.

## Initial dissolution profile and kinetics of glasses for bio applications

**Dagmar Galusková<sup>1</sup>, Hana Kaňková<sup>1</sup>, Anna Švančárková<sup>1</sup>, Si Chen<sup>1</sup> and Dušan Galusek<sup>1</sup>**

<sup>1</sup>Centre for Functional and Surface Functionalized Glass,  
Alexander Dubček University of Trenčín, Študentská 2, 91150 Trenčín, Slovakia  
(dagmar.galusko@tuni.sk)

### ABSTRACT

The dissolution studies of bioactive glasses and ceramics are usually performed at the static conditions and evaluation of dissolution rely on data from the following time interval 1, 3, 7 and 14 days. The compositional changes of immersion solution in first minutes and hours of biomaterial leaching are usually not addressed. However, the early stage of dissolution provides valuable information about leaching kinetics and represent one of the most important part in case of controlled release of ions into the aqueous solution. Solutions simulating body fluid (SBF) are usually buffered with TRIS to maintain the pH ~7 and are used as a leaching media for prediction of dissolution behavior of bioactive glasses [1][2].

A continuous flow measurement recording the ion release online (*inline test*) with the optical emission spectrometer with inductively coupled plasma (ICP OES) has been studied with respect to the initial dissolution. The fresh leaching solution was pumped continuously through a cell, filled with powder glass sample reflecting the composition of Bioglass 45S5 23Na<sub>2</sub>O, 23CaO, 6P<sub>2</sub>O<sub>5</sub>, 48SiO<sub>2</sub> (wt%) and with addition of boron and zinc as ions with possible therapeutic effect. The intensities of measured signals for particular ions are quantified by comparison with calibration standards of known concentration.

The corrosion cell was tempered at the temperature 37°C in thermostatic bath. The concentration of dissolved ions and pH of input SB solution are constant during inline test, the ions released from the glass powder are measured on the output of the reaction cell. The concentration above detection limit is included in calculation and the amount of released ions normalized to their content in glass will be discussed for evaluation of mechanisms of dissolution of bioactive glasses. The limits of detection of studied therapeutic ions were published in [2]. Both type of tests need to be included in testing the bio-response. The static test give answer for apatite formation ability of tested bioactive glass system, whereas the flow through and inline tests address the initial release of ions. The initial concentration of metals released to human body could trigger therapeutic healing or could become toxic for cells.

### EXPERIMENTAL PART

The static tests were performed only in SBF prepared according [1]. 10 mg of sample was leached in 15 ml SBF. The tubes with sample and leaching solution were placed into the thermostatic bath set to 37°C for 1, 3 and 7 days. After the test the final solution was filtered to separate undissolved particles and its elemental chemical composition was measured by ICP OES.

Normalized leached amount of ions was calculated applying the following equation (1):

$$NL_i(t) = \frac{c_i * V}{w_i * m} \quad (1)$$

where  $c_i$  is concentration of element measured in leaching solution in time and subtracted from the blank (concentration of element in the input SBF solution),  $V$  is a volume of the leaching solution,  $w_i$  is a weight fraction of element  $i$  in sample,  $m$  is weight of sample.

For the flow-through inline test the thermostatic bath, corrosion cell, peristaltic pump and tubing were assembled and connected directly to the introduction system of the optical emission spectrometer (ICP OES 5100 SVDV, Agilent). Internal standard scandium (10 mg/L) was included in inline sampling in order to deal with non-spectral interferences.

Dissolution of borosilicate glass with different content of boron and cobalt prepared in FunGlass Centre by dr. Si Chen were tested. As a leaching medium were used simulated body fluid (SBF, pH 7.4) that is frequently used in leaching bioactivity tests, TRIS (tris-(hydroxymethyl)

aminomethane) buffer set pH to the value 7.4 at the temperature 36.5°C.

Inline tests were conducted with 100 mg of sample soaked in approx. 1 mL volume cell, through which continuously flew fresh leaching solution at the temperature held constant at  $37 \pm 1$  °C. Concentration of Ca, B, Co, P, Si as function of time was directly monitored using ICP software. Data from dissolution of sample were monitored every 2 minutes for 1.5 hours. The total amount of leached elements ( $NL_i$ ) is determined by the following equation (2) as cumulative release of particular ion:

$$NL_i(t) = c_i \frac{F}{w_i * m} \Delta t + NL_i^{t-\Delta t} \quad (2),$$

where  $c_i$  is concentration of particular leached element in time  $t$ ,  $F$  is the flow rate,  $w_i$  is weight ratio of element  $i$  in sample. Values of the initial leaching rate may be evaluated from the experimental time dependencies of  $NL_i$  [3].

## RESULTS AND DISCUSSION

On the Fig. 1 is plotted the release of cobalt under static and dynamic (*inline measurement of Co*) condition for the initial stage of glass dissolution. The ion is released linearly already in the first minutes and after one day the rate decreases to zero. The slope of linear curve detected from inline dynamic tests differs from the slope acquired by plotting the static tests from zero time. The element concentration measured at the static conditions were constant for the whole time interval. It means that equilibrium was already achieved during the first day.

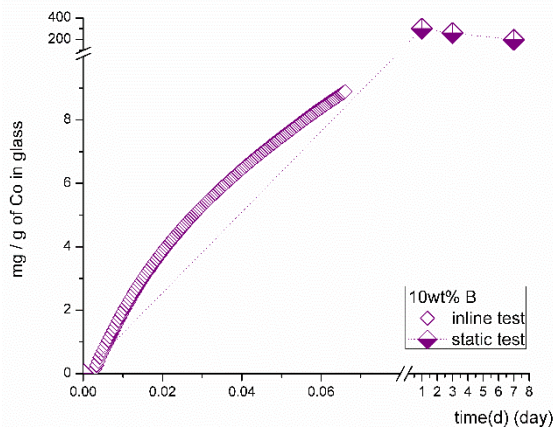


Fig. 1: Release of cobalt from borosilicate glass in the initial time of immersion to SB fluid under static and dynamic (inline) test conditions at 37°C.

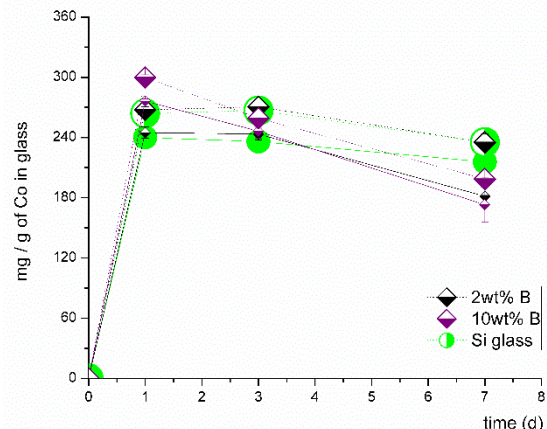


Fig. 2: Release of cobalt from borosilicate glass of various composition to SB fluid under static conditions at 37°C.

Evaluation of obtained data based on concentration is indicative for how much ion is released to human environment. Therefore, the information obtained from inline minute tests addresses the initial dissolution performance of material in SB fluid, such information can become crucial in respect of cytotoxicity. However, evaluation of data based on concentration do not provide relevant information about mechanism of dissolution of glass especially with different structural and compositional characteristics. The studied system of borosilicate glass with different addition of cobalt and boron dissolved in the comparable mechanism based on evaluation of data from the static test (Fig. 2).

## CONCLUSIONS

Both type of tests need to be included in testing the bio-response. The static test give answer for apatite formation ability of tested bioactive glass system, whereas the flow through and inline tests address the initial release of ions. The initial concentration of metals released to human body could trigger therapeutic healing or could become toxic for cells. To discuss mechanism of dissolution of glasses of different composition and structure, the amounts of released ions normalized to their content in studied system need to be considered according to either static eq. (1) or dynamic eq. (2) conditions.

**Keywords:** bioactive glass, dynamic test, SBF,

## Acknowledgment:



This item is a part of dissemination activities of project FunGlass. This project has received funding from the European Union's Horizon 2020 research and innovation programme under grant agreement No 739566.

This presentation was also created in the frame of the project Centre for Functional and Surface Functionalized Glass (CEGLASS), ITMS code is 313011R453, operational program Research and innovation, co-funded from European Regional Development Fund.

## References:

- [1] Kokubo T., Takadama H. How useful is SBF in predicting in vivo bone bioactivity? *Biomaterials* 27, 2907–15 (2006)
- [2] Blochberger M., Hupa L., Brauer D.S., Influence of zinc and magnesium substitution on ion release from 45S5 at physiological and acidic pH, *Biomed. Glass.*, 1 (2015)
- [3] Galusková D., Kaňková H., Inline measurement of leachates from bioglass immersion tests, book of abstracts, FG school, 38-40, T. Teplice 2018
- [4] Mišíková L., Galusková D., Corrosion of E-glass fibers, security factor of nuclear power plants, *Ceramics-Silikáty* 50 (2006)

## Multi-targeted B and Co co-doped bioactive glass for angiogenesis

**Si Chen<sup>1,3</sup>, Martin Michálek<sup>1,3</sup>, Dagmar Galusková<sup>2</sup>, Monika Michálková<sup>2</sup>, Peter Švančárek<sup>2</sup>, Ali Talimian<sup>2</sup>, Hana Kaňková<sup>1</sup>, Jozef Kraxner<sup>1</sup>, Liliana Liverani<sup>3</sup>, Kai Zeng<sup>3</sup>, Dušan Galusek<sup>2</sup>, Aldo R. Boccaccini<sup>3</sup>**

<sup>1</sup> Centre for Functional and Surface Functionalized Glass, TnU AD, Trenčín, Slovakia  
(E-mail: si.chen@tnuni.sk)

<sup>2</sup> Joint Glass Centre of the IIC SAS, TnU AD and FChFT STU, Centre for Functional and Surface Functionalized Glass, TnU AD, Trenčín, Slovakia

<sup>3</sup> Institute of Biomaterials, University of Erlangen-Nuremberg, Erlangen, Germany

### ABSTRACT

In tissue regeneration area, vascularization is necessary and important to keep adequate blood supply to maintain the survival and growth of new tissue. Because the diffusion distance of nutrients and oxygen for cell survival is limited to 150-200  $\mu\text{m}$ , the viability of the cells at the center of the scaffold is severely hampered [1]. Generally, the tissue layers on the scaffold surface is not thicker than 5 mm, and in the centre of the scaffold, cell density tends to be low and necrosis may occur [1]. Therefore, appropriate angiogenesis for adequate blood supply is necessary and important. Several biomolecules (vascular endothelial growth factor (VEGF) [2] and basic fibroblast growth factor (bFGF) [3]), as well as metal ions (copper (Cu) [4], cobalt (Co) [5], strontium (Sr) [6], magnesium (Mg) [7], B [8] and calcium (Ca) [9]) have been already used to promote angiogenesis. In the area of ions-induced angiogenesis, single ion including Cu, Co, Sr, Mg, B and Ca has been extensively investigated: their effectiveness on angiogenesis was demonstrated [4-9]. In the past decade, B has been increasingly used in bioactive materials to promote angiogenesis, exhibiting positive effect on neovascularization. B potently activates the MAPK signalling pathway to markedly enhance the secretion of VEGF, interleukin 6 (IL-6) and bFGF [8, 10, 11] which as the pro-angiogenic cytokines would stimulate the angiogenic response [12, 13]. Co as an essential element in human physiology can also promote angiogenesis, albeit in a different way.  $\text{Co}^{2+}$  ion is a well-established chemical inducer of HIF-1 $\alpha$  which elicits a significant hypoxic cascade [14] including VEGF secretion, identified as a key regulator in angiogenesis [15, 16]. It is worth noting that B and Co promote angiogenesis through two different targets: the MAPK signalling pathway and hypoxia pathway. However, the synergy of multi-target on angiogenesis promotion is rarely investigated. Therefore, in this story, B and Co were co-doped bioactive glass in order to verify possible synergistic effect of these elements on angiogenesis promotion through multi-target way.

In first part, the synergy of multi-targeted B and Co were co-doped bioactive glass on angiogenesis promotion was directly investigated. The 45S5 bioactive glass co-doped with B and Co was prepared by conventional melt quenching method: synergistic effect of the two co-doping elements on angiogenesis promotion in two different targets is expected. ATR-Fourier transform infrared spectroscopy, energy-dispersive X-ray spectroscopy and inductively coupled plasma-optical emission spectrometry were used to characterize the composition, element distribution and ions release of the samples. Results showed that the compositions of all samples are almost consistent with the design, and all elements in samples are homogeneously distributed. Different content of B and Co implies different release rates of these elements. The samples showed bioactivity after immersion in simulated body fluid. The 1% and 0.1% extracts of all samples did not show any cytotoxicity to MG-63 and ST-2 cells. Compared with single B and Co, B and Co co-doped sample more strongly increases the secretion of vascular

endothelial growth factor from ST-2 cells, which supports and confirms the synergistic effect of multi-targeted B and Co co-doping on angiogenesis.

In second part, the tissue engineering scaffold embedding multi-targeted B and Co were co-doped bioactive glass was fabricated for multi-targeted promotion of angiogenesis. The polycaprolactone (PCL) fiber mats embedding multi-targeted B and Co co-doped bioactive glass nanoparticles were fabricated as a tissue regeneration scaffold especially for angiogenesis. B and Co co-doped bioactive glass nanoparticles were successfully prepared with well-defined sphere shape by sol-gel method. B and Co were indeed doped into the nanoparticles. The PCL fiber mats embedding multi-targeted B and Co co-doped bioactive glass nanoparticles were successfully fabricated with clear fibrous and free-beads shape by electrospinning. The Young's moduli of the PCL fiber mats with nanoparticles were similar with the pure PCL fiber mats and suitable to support deformation in scaffolds for soft tissue. The mats also showed a biocompatibility to ST-2 cells. The PCL fiber mats with high content of B and Co promoted the secretion of vascular endothelial growth factor in comparison with the PCL fiber mats with low content of B and Co and without B and Co which demonstrated its potential as a tissue regeneration scaffold material for angiogenesis.

**Keywords:** multi-target, synergistic effect, angiogenesis, bioactive glass, boron, cobalt, soft tissue regeneration

#### Acknowledgment:



This item is a part of dissemination activities of project [FunGlass](#). This project has received funding from the European Union's Horizon 2020 research and innovation programme under grant agreement No 739566.

#### References:

- [1] Laschke M W, Harder Y, Amon M, et al. Angiogenesis in tissue engineering: breathing life into constructed tissue substitutes. *Tissue engineering*, 2006, 12(8): 2093-2104.
- [2] Street J, Bao M, Bunting S, et al. Vascular endothelial growth factor stimulates bone repair by promoting angiogenesis and bone turnover. *Proceedings of the National Academy of Sciences*, 2002, 99(15): 9656-9661.
- [3] Schnettler R, Alt V, Dingeldein E, et al. Bone ingrowth in bFGF-coated hydroxyapatite ceramic implants. *Biomaterials*, 2003, 24(25): 4603-4608.
- [4] Stähli C, James-Bhasin M, Hoppe A, et al. Effect of ion release from Cu-doped 45S5 Bioglass® on 3D endothelial cell Morphogenesis. *Acta biomaterialia*, 2015, 19: 15-22.
- [5] Wu C, Zhou Y, Fan W, et al. Hypoxia-mimicking mesoporous bioactive glass scaffolds with controllable cobalt ion release for bone tissue engineering. *Biomaterials*, 2012, 33(7): 2076-2085.
- [6] Mao L, Xia L, Chang J, et al. The synergistic effects of Sr and Si bioactive ions on osteogenesis, osteoclastogenesis and angiogenesis for osteoporotic bone regeneration. *Acta Biomaterialia*, 2017, 61: 217-232.
- [7] Yu Y, Jin G, Xue Y, et al. Multifunctions of dual Zn/Mg ion co-implanted titanium on osteogenesis, angiogenesis and bacteria inhibition for dental implants. *Acta biomaterialia*, 2017, 49: 590-603.
- [8] Durand L A H, Góngora A, López J M P, et al. In vitro endothelial cell response to ionic dissolution products from boron-doped bioactive glass in the SiO<sub>2</sub>-CaO-P<sub>2</sub>O<sub>5</sub>-Na<sub>2</sub>O system. *Journal of Materials Chemistry B*, 2014, 2(43): 7620-7630.
- [9] Oliveira H, Catros S, Castano O, et al. The proangiogenic potential of a novel calcium releasing composite biomaterial: Orthotopic in vivo evaluation. *Acta Biomaterialia*, 2017, 54: 377-385.
- [10] Presta M, Dell'Era P, Mitola S, et al. Fibroblast growth factor/fibroblast growth factor receptor system in angiogenesis. *Cytokine & growth factor reviews*, 2005, 16(2): 159-178.
- [11] Durand L A H, Vargas G E, Romero N M, et al. Angiogenic effects of ionic dissolution products released from a boron-doped 45S5 bioactive glass. *Journal of Materials Chemistry B*, 2015, 3(6): 1142-1148.
- [12] Park M, Li Q, Shcheynikov N, et al. NaBC1 is a ubiquitous electrogenic Na<sup>+</sup>-coupled borate transporter essential for cellular boron homeostasis and cell growth and proliferation. *Molecular cell*, 2004, 16(3): 331-341.
- [13] Garbers C, Hermanns H M, Schaper F, et al. Plasticity and cross-talk of interleukin 6-type cytokines. *Cytokine & growth factor reviews*, 2012, 23(3): 85-97.
- [14] Pacary E, Legros H, Valable S, et al. Synergistic effects of CoCl<sub>2</sub> and ROCK inhibition on mesenchymal stem cell differentiation into neuron-like cells. *Journal of cell science*, 2006, 119(13): 2667-2678.
- [15] Ferrara N, Davis-Smyth T. The biology of vascular endothelial growth factor. *Endocrine reviews*, 1997, 18(1): 4-25.
- [16] Lode A, Wolf-Brandstetter C, Reinstorf A, et al. Calcium phosphate bone cements, functionalized with VEGF: release kinetics and biological activity. *Journal of Biomedical Materials Research Part A*, 2007, 81(2): 474-483.

## Electrospun polycaprolactone membranes doped with bioactive glass nanoparticles for tissue regeneration

Z. Neščáková<sup>1</sup>, L. Liverani<sup>2</sup>, K. Zheng<sup>2</sup>, M. Michálek<sup>1</sup>, D. Galusek<sup>1</sup>, A.R. Boccaccini<sup>2</sup>

<sup>1</sup> FunGlass - Centre for Functional and Surface Functionalized Glass, Alexander Dubček University of Trenčín, Slovakia (zuzana.nescakova@tnuni.sk)

<sup>2</sup> Institute of Biomaterials, Department of Materials Science and Engineering, University of Erlangen-Nuremberg, Germany

### ABSTRACT

Bioactive glasses (BGs) continue to attract interest for applications in hard tissue engineering for replacement, regeneration and repair bone and teeth. Their application possibilities have covered also the area of soft tissue engineering (angiogenesis, cardiac, lung, nerve, gastrointestinal tissue regeneration) and wound healing<sup>[1]</sup>. BGs are often incorporated into a polymeric matrix to produce composite which can act as a scaffold or nets for cell adhesion. Biodegradable composite offers a suitable environment for later differentiation, proliferation of the cells and stimulate direct tissue formation *in situ*<sup>[2]</sup>. The main aim of this work is synthesis of bioactive glass particles, which are subsequently incorporated to PCL-fibres to create multifunctional membranes for tissue regeneration. Well dispersed spherical nano-sized mesoporous glasses ( $130 \pm 10$  nm) based on the binary SiO<sub>2</sub>-CaO system were synthesized by using a microemulsion-assisted sol-gel approach<sup>[3]</sup>. After comprehensive characterization (SEM-EDS, XRD, FTIR, TEM, BET, bioactivity and cell viability tests), BGs were used for nanocomposite fabrication. The fibre membranes were fabricated by electrospinning method. Biodegradable poly  $\epsilon$ - caprolactone were used as a polymer matrix. The small size of BGs particles allowed their incorporation into the fibers all over the fiber length. After immersion in simulated body fluids the membranes showed ability to form hydroxyapatite. The obtained bioactive materials have the potential for application in regenerative medicine.

**Keywords:** bioactive glass, electrospun membranes;

### Acknowledgment:



This publication was created in the frame of the project Centre for Functional and Surface Functionalized Glass (CEGLASS), ITMS code is 313011R453, operational program Research and innovation, co-funded from European Regional Development Fund.

### References:

- [1] V. Miguez-Pacheco, L. L. Hench, and A. R. Boccaccini, 'Bioactive glasses beyond bone and teeth: Emerging applications in contact with soft tissues', *Acta Biomater.*, vol. 13, pp. 1–15, 2015.
- [2] K. Rezwan, Q. Z. Chen, J. J. Blaker, and A. Roberto, 'Biodegradable and bioactive porous polymer / inorganic composite scaffolds for bone tissue engineering', *Biomaterials*, vol. 27, pp. 3413–3431, 2006.
- [3] Q. Liang, Q. Hu, G. Miao, B. Yuan, and X. Chen, 'A facile synthesis of novel mesoporous bioactive glass nanoparticles with various morphologies and tunable mesostructure by sacrificial liquid template method', *Mater. Lett.*, vol. 148, pp. 45–49, 2015.

## Dissolution process of Bioglass 45S5 in physiological and acidic environment

**A.Švančárková<sup>1,2</sup>, D.Galusková<sup>1</sup>, H. Kaňková<sup>1</sup>, M. Michálek<sup>1</sup>, D.Galusek<sup>1</sup>**

<sup>1</sup> FunGlass, Centre for Functional and Surface Functionalized Glass, Department of Biomaterials, Alexander Dubček University of Trenčín, Študentská 2, 911 50 Trenčín, Slovakia

(E-mail: annasvancarkova@tuni.sk)

<sup>2</sup>Faculty of Chemical and Food Technology STU, Radlinského 9, 812 37 Bratislava, Slovakia

### ABSTRACT

The 45S5 Bioglass (BG) prepared by Hench with weight composition 45% SiO<sub>2</sub>, 24.5% CaO, 24.5 Na<sub>2</sub>O and 6% P<sub>2</sub>O<sub>5</sub> is a bioactive material that stimulates bone repair. In aqueous environment, this material undergoes a series of reactions to create a surface layer of hydroxy-apatite (HA) and hydroxy-carbonate apatite. The incorporation of ions in BG can enhance the therapeutic effects of the material.

In this study, the effect of different solution media to the corrosion behavior of 45S5 bioactive glass (BG) and 45S5 bioglass doped with boron (4 wt%) or zinc (4 wt%) was investigated. In vitro tests were carried out in simulated body fluid (pH 7.4) and acetic acid buffered with sodium acetate (pH 4) solution simulating inflammatory environment.

Glass powders with theoretical composition (in wt%) described in Tab.1. were fabricated by conventional melting. The prepared bulk glass was crushed and sieved to achieve particle size  $\leq 25\mu\text{m}$

Tab.1: Comparison of the theoretical and experimental composition (ICP OES analyses of samples decomposed in mineral acids) of tested bioactive glass in wt%.

wt%	45S5		45S5+4B		45S5+4Zn	
	Theor. Comp.	Experim. comp.	Theor. Comp.	Experim.c omp.	Theor. Comp.	Experim.c omp.
SiO <sub>2</sub>	45	42.0±2.1*	44.5	42.9±1.9*	44.5	42.3±2.4*
P <sub>2</sub> O <sub>5</sub>	6	6.1±1.2	5.9	8.5±2.7	5.9	9.0±3.1
CaO	24.5	23.5±2.3	21.4	21.7±1.5	21.4	21.7±1.0
Na <sub>2</sub> O	24.5	23.4±1.8	24.2	23.1±0.8	24.2	23.3±2.1
ZnO	-	-	-	-	4	3.7±0.8
B <sub>2</sub> O <sub>5</sub>	-	-	4	3.9±0.6	-	-

\*normalized to 100%

Dissolution studies were performed at the static conditions in the neutral and acidic environment.

The 35 mg of glass powder was immersed in 25 ml of solution at 37°C for 1, 2, 4, 8 and 24 hours. After each time period, composition of corrosion solutions were analyzed using inductively coupled plasma optical emission spectrometer (ICP-OES, Agilent 5100). Each experiment was performed in three parallels. The amount of released ions (in mg/L) were presented as normalized leached values of the respective element -NL<sub>i</sub> (in mg of element/g of

element in initial powder).

NL values were calculated based using the following (1):

$$NL_i = \frac{c_i * V}{w_i * m_s}, \quad (1)$$

where V is volume of corrosion medium,  $w_i$  - mass fraction of an element in the sample,  $c_i$  - concentration of an element i in the sample and  $m_s$  is weight of the initial powder.

In SBF solution, silicon concentration increased in all materials rapidly during the first 1-2 h (Fig.1). This initial faster release of Si occurs during the second stage of the deposition of HA layer on the surface of BG. During this second stage Si–O–Si bonds are broken and soluble silica is released to the solution. The reason for decrease of phosphorus in solution is the strong adsorption of phosphorus ions from SBF solution to the glass surface. Adsorption of phosphorus ions from SBF is due to solution supersaturation necessary to form Ca–P rich reaction layer (the fourth stage of the deposition of HA layer). For samples 45S5+Zn and 45S5+B we did not observe any significant decrease of phosphorus content in corrosion solutions. The reason can be higher content of phosphorus in this untreated samples (Tab.1), also it is not necessary to pump so much ions of phosphorus for creating HA layer from the SBF. In SBF, elution of ions was the slowest in 45S5+Zn. In this material, the release of zinc as a potential antibacterial inhibitor was meeting the limit of quantification.

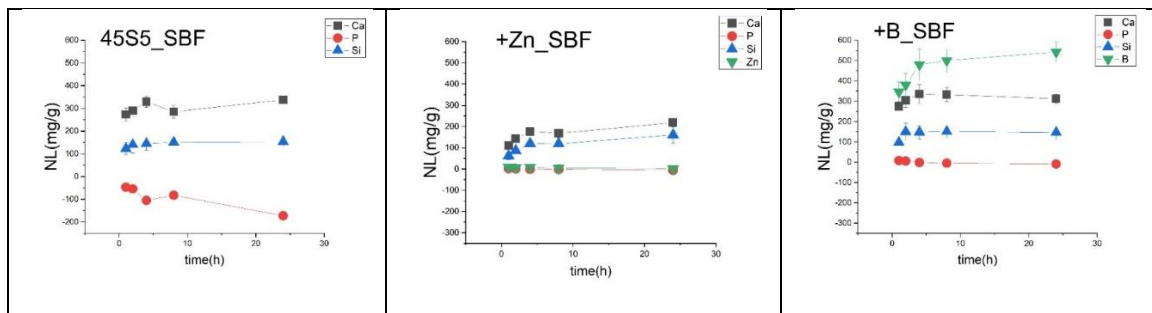


Fig.1: Time dependence of the ions released from the studied glass systems into SBF of 45S5, 45S5+4Zn and 45S5+B.

In HAc/NaAc buffer, all tested bioglasses showed fast release of ions (Fig.2). While the silicate network was relatively stable in acidic environment, and release of Si was relatively slow, the network modifiers Na, Ca, P and Zn or B leached out from the material very quickly. This behaviour is potentially favorable for curing or stopping inflammation process in the body through rapid dissolution of bioactive glass and release of zinc to fight bacterial infection. Incorporation of zinc in the glass structure increases its network connectivity [1]. However when zinc is leached out in acidic environment already in the early stage of the dissolution process, the residual glass tends to dissolve rapidly

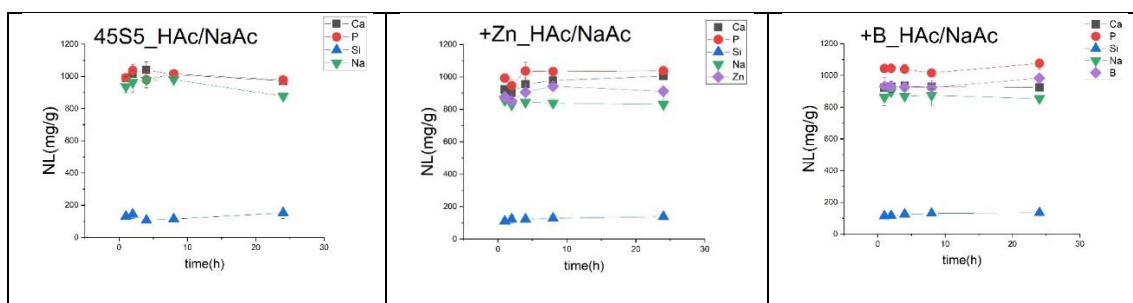


Fig.2: Time dependence of the ions released from the studied glass systems in acetic acid/sodium acetate buffer (pH4) of 45S5, 45S5+4Zn and 45S5+B.

**Keywords:** bioactive glass, dissolution, acetic acid/sodium acetate buffer, simulated body fluid

## LITERATURE

[1] Blochberger, M., Hupa, L., Brauer, D.S. Influence of zinc and magnesium substitution on ion release from Bioglass 45S5 at physiological and acidic pH, *Biomed.Glasses* 1 (2015) 93-107.

## Acknowledgment:



This paper is a part of dissemination activities of project [FunGlass](#).  
This project has received funding from the European Union's Horizon 2020 research and innovation programme under grant agreement No 739566.  
This presentation was also created in the frame of the project Centre for Functional and Surface Functionalized Glass (CEGLASS), ITMS code is 313011R453, operational program Research and innovation, co-funded from European Regional Development Fund.